# A 17-year dataset of surface water fugacity of $CO_2$, along with calculated pH, aragonite saturation state, and air-sea $CO_2$ fluxes in the Northern Caribbean Sea

Rik Wanninkhof[1], Denis Pierrot[1,2], Kevin Sullivan[1,2], Leticia Barbero[1,2], and Joaquin Triñanes[1,2,3]

[1]Atlantic Oceanographic and Meteorological Laboratory (AOML), NOAA, 4301 Rickenbacker Causeway, Miami, FL 33149 USA

[2]Cooperative Institute for Marine and Atmospheric Studies, Rosenstiel School of Marine and Atmospheric Science, University of Miami, 4600 Rickenbacker Causeway, Miami, FL 33149 USA

[3]Laboratory of Systems, Technological Research Institute, Universidad de Santiago de Compostela, Campus Universitario Sur, Santiago de Compostela, 15782, Spain

*Correspondence to*: Rik Wanninkhof (rik.wanninkhof@noaa.gov)

**Abstract.** A high-quality dataset of surface water partial pressure/fugacity of $CO_2$ ($pCO_{2w}$/$fCO_{2w}$)[1], comprised of over a million observations, and derived products are presented for the Northern Caribbean Sea covering the timespan from 2002 through 2018. Prior to installation of automated $pCO_2$ systems on cruise ships of the Royal Caribbean Cruise Lines and subsidiaries, very limited surface water carbon data were available in this region. With this observational program, the Northern Caribbean Sea has now become one of the best sampled regions for $pCO_2$ of the world's ocean. The dataset, and derived quantities are binned and averaged on a 1-degree monthly grid and are available at http://accession.nodc.noaa.gov/0207749, https://doi.org/10.25921/2swk-9w56 (Wanninkhof et al., 2019a). The derived quantities include total alkalinity (TA), acidity (pH), aragonite saturation state ($\Omega_{Ar}$) and air-sea $CO_2$ flux, and cover the region from 15˚ N to 28˚ N and 88˚ W to 62˚ W. The gridded data and products are used for determination of status and trends of ocean acidification, for quantifying air-sea $CO_2$ fluxes, and for ground truthing models. Methodologies to derive the TA, pH and $\Omega_{Ar}$, and to calculate the fluxes from $fCO_{2w}$ temperature and salinity are described.

## Introduction

Over the past 20 years a rapidly expanding program of measurements of surface water partial pressure of carbon dioxide ($pCO_{2w}$)[1], or the fugacity of $CO_2$ ($fCO_{2w}$)[1] has provided data to determine air-sea $CO_2$ fluxes and rates of ocean acidification on local to global scales (e.g. Boutin et al., 2008; Degrandpre et al., 2002; Evans et al. 2015; Schuster et al., 2012; Takahashi et al., 2014; Wanninkhof et al. 2019 a, b). Marginal seas, that historically had a dearth of measurements, have been targeted for increased observations. Through an industry, academic, and federal partnership between the U.S. National Oceanic and Atmospheric Administration (NOAA), Royal Caribbean Cruise Lines (RCCL), and the University of Miami, cruise ships were outfitted with automated surface water $pCO_2$ systems, also called underway $pCO_2$ systems (Pierrot et al., 2009). In 2002, the RCCL ship *Explorer of the Seas* (*EoS*) was equipped with an underway $pCO_2$ setup providing observations on alternating weekly transects from Miami, FL to the Northeastern and Northwestern Caribbean. In 2015, the *EoS* was repositioned out of the Atlantic and the *Celebrity Equinox* (*Eqnx*) was outfitted with an underway $pCO_2$ system. Additionally, an underway $pCO_2$ system was installed on the *Allure of the Seas (ALoS)* in 2016. The *Eqnx* and *ALoS* covered similar transects as the *EoS* but on more irregular and seasonal basis. A total of 582 cruises covered the region from 2002 through 2018. A map of all cruise tracks is shown in Figure 1. The number of cruises per year covering the Caribbean Sea and adjacent Western Atlantic are provided in Figure 2. There are fewer cruises in the middle part of the record when the *EoS* was diverted to other routes outside the area, and eventually repositioned.

[1] $fCO_2$ is the $pCO_2$ corrected for the non-ideal behavior of $CO_2$ (Weiss 1974). In surface water $fCO_{2w} \approx 0.997\ pCO_{2w}$

The surface water $pCO_2$ observational dataset and derived products including total alkalinity (TA), acidity (pH), aragonite saturation state ($\Omega_{Ar}$), and air-sea $CO_2$ flux are of importance for determining the anthropogenic carbon uptake, and to assess trends and impacts of ocean acidification. The observational data are provided to the global surface ocean carbon atlas (SOCAT) (Bakker et al., 2016) and global $CO_2$ climatology (Takahashi et al., 2009; 2018). These data are the main source of $fCO_2$ observations available in the region, and the high frequency of measurements provides a seasonally resolved picture of changing $fCO_{2w}$. This effort has made the Northern Caribbean one of the few places in the world's ocean where such regional observational density has been established. The data and mapped products are interpreted in Wanninkhof et al. (2019b) who show large decadal changes in trends of surface water $fCO_2$ and associated changes in air-sea $CO_2$ fluxes.

The data from the first part of this record form the basis of the Caribbean ocean acidification product suite that maps ocean acidification conditions in the Caribbean (Gledhill et al., 2008; https://www.coral.noaa.gov/accrete/oaps.html; https://cwcgom.aoml.noaa.gov/erddap/griddap/miamiacidification.graph). The large, high quality, and well-resolved dataset is also used to validate models (Gomez et al., 2020).

For optimal application, datasets and associated data products are fully documented here, and are readily accessible according to the findable, accessible, interoperable and reusable (FAIR) principles (Wilkinson et al., 2016). In addition, the data underwent substantial quality control by our group and through the SOCAT quality control and check procedures. The documentation of the cruises, the sampling methodology, and data reduction techniques are presented in brief. This is followed by a description of the approaches to calculate the different inorganic carbon system parameters. The procedure is to bin and average the $fCO_{2w}$ on a 1˚ by 1˚ grid on monthly scales, referred to as gridded observations. Then the so-called second inorganic carbon system parameter is calculated. We estimate the total alkalinity (TA) based on robust relationships of TA with salinity (Cai et al., 2010; Takahashi et al., 2014; Lee et al., 2006; Millero et al., 1998), and use a software program CO2SYS (Pierrot et al., 2006) to calculate the other inorganic carbon system parameters of interest, in this case pH and $\Omega_{Ar}$. These data products are presented at monthly scales binned and averaged on a 1˚ by 1˚ grid, referred to as gridded products. Annual multi-linear regressions (MLR) are developed between the gridded $fCO_{2w}$ data, and sea surface temperature (SST), sea surface salinity (SSS), location (latitude (Lat) and longitude (Lon)), and mixed layer depth as independent variables. These regressions are applied at monthly and 1˚ by 1˚ spatial resolution to the region between 15˚ N and 28˚ N, and 88˚ W and 62˚ W using remotely sensed or modeled independent variables, and used to calculate air-sea $CO_2$ fluxes. These calculated parameters are called gridded mapped products. The procedures and datasets, including uncertainty analyses, and tables of column headers of the product created are provided below.

## 1 Observations

The observational program is described in terms of the ships, voyages, and instrumentation. The ships predominantly sailed in the Caribbean Sea, but also had tracks outside the region, including in the Northeast of the USA, to Bermuda and in the Mediterranean. The description of operations, data, and products presented here cover the Northern Caribbean Sea and Western

Atlantic, north of the Caribbean islands chain covering the region from 15˚ N to 28˚ N and -62˚ to -88˚ (= 62˚ W to 88˚ W) (Fig. 1). The homeports of the ships, where passengers embark and disembark, are Miami and Fort Lauderdale, FL. The *Explorer of the Seas (EoS*) changed homeport from Miami, FL to Cape Liberty Cruise Port, NJ in 2008, and changed its routes at that point to include cruises with Bermuda as a port of call. In 2015 the *EoS* was repositioned to the Pacific and the underway $pCO_2$ system was removed. From 2015 onward the *Celebrity Equinox (Eqnx)* and from 2016 onward the *Allure of the Seas* (*ALoS)* covered the area. The *Eqnx* spent the summers of 2015 and 2016 in the Mediterranean, causing seasonal data gaps in the Caribbean.

### 1.2 Cruises

The *EoS* had 331 cruises from 2002 to 2015; the *Eqnx* completed 135 cruises from 2015 through 2018; and the *ALoS* performed 116 cruises in the study area from 2016 through 2018. Temporal coverage over the 17 years shows at least bi-weekly occupations at the beginning of the record from 2002 to 2007, and at the end from 2014 through 2018, with fewer occupations in the years in between (Fig. 2). The cruises lasted between 7 and 14 days, and made about a half a dozen ports of call. The ships generally were in port from early morning to late afternoon, and transited between ports at night, except for long runs (e.g., from Miami to San Juan) when the ship sailed continuously for several days. Ports are listed in the metadata accompanying the original data.

The systems were installed in different locations for the three ships, but each had a dedicated seawater intake near the bow. The *EoS* had an intake in the bow thruster tube (≈3 m depth) that was non-optimal due to bubble entrainment during bow thruster operations and heavy seas. These observations have been culled from the datasets. The *ALoS* and *Eqnx* had their intake at ≈5 m depth, but forward of the bow thruster and had fewer issues with bubble entrainment. On the *EoS,* the underway $pCO_2$ instrument was initially in a dedicated science laboratory built for purpose on the ship, and located amidships about 100 m from the intake. In 2008, a new system was placed in the engineering space closer to the bow with no apparent change in performance. For the *ALoS* and *Eqnx,* the instruments were near the bow intake in the engineering space, about 5 m from the intake. The *EoS* had an air intake mounted on a mast at the forward most point of the main deck in August of 2008. The *Eqnx* had an air intake near the bow one level below the main deck since the initial installation in March 2015. The underway $pCO_2$ systems on these ships made marine boundary layer (MBL) air observations ($xCO_{2a}$) as described in Wanninkhof 2019b but these are not used in the data products presented. Typical cruise speeds were 22 knots which, with sampling every 2.5 minutes, yielded a $fCO_{2w}$ sample approximately every 1.7 km except for 35 minutes every 4.5 hours when four calibration gases, and a $CO_2$-free reference gas were analyzed, followed by 5 atmospheric $CO_2$ measurements for the ships with air intakes. This created a gap of 24 km (≈1/4˚) without $fCO_{2w}$ measurements

### 1.3 Instrumentation

#### 1.3.1 $pCO_2$ system

The instrumentation is based on a community design described in Pierrot et al. (2009). The instruments were manufactured by General Oceanics Inc., and for the cruises described here, they have performed to high accuracy specifications at described in Wanninkhof (2013). The surface water drawn from the intake at about 4 l $min^{-1}$ went through a 1.1 l sprayhead equilibrator with a water volume of 0.5 l and a headspace of 0.6 l. The spray and agitation caused the $CO_2$ in the headspace to equilibrate with the $CO_2$ in water with a response time of about 2 minutes (Pierrot et al., 2009; Web et al., 2016). Thus, the air in the headspace reached 99.8 % equilibration in 12 minutes. As the air is recirculated and surface waters were relatively homogeneous on hourly timescales, 100.0 % equilibration was assumed. The four calibration gases supplied by the global monitoring division of the environmental science research laboratory of NOAA (GMD/ ESRL/NOAA) were traceable to the WMO $CO_2$ mole fraction scale. The $CO_2$ concentrations of the standards spanned the range of surface water values encountered along the ship tracks (≈ 280- 480 ppm).

The gas entering the analyzer was dried by passing it through a thermo-electric cooler at 5˚ C and a PermaPure drier. The standards did not contain water vapor. The air and equilibrator headspace analyses typically had about 10 % or less humidity. Every 27 hours the $CO_2$ signal of the LICOR model 6262 infrared analyzer was zeroed with the dry $CO_2$-free air and spanned with the highest standard. The water vapor channel was zeroed if it showed reading of greater than 0.5 millimol/mol for the dry $CO_2$-free air. The water vapor channel values are used for a minor correction to the xCO2, and any inaccuracy in the $H_2O$ results in 0.5 ppm change in the analyzer output of dry mole fraction of $CO_2$ ($xCO_2$ in parts per million, ppm). $xCO_2$ as calculated and output by the analyzer, based on measured $CO_2$ and water vapor levels, were recorded. The seawater circulation in the systems was automatically turned off when the ships entered port, and back-flushed with fresh water removing particles from the inline water filter and thereby alleviating clogging issues in the filter and reducing biofouling of water lines, filter and equilibrator.

Data from the *ALoS* and *Eqnx* were transmitted to shore daily and displayed online in graphical format at https://www.aoml.noaa.gov/ocd/ocdweb/allure/allure_realtime.html and https://www.aoml.noaa.gov/ocd/ocdweb/equinox/equinox_realtime.html, respectively. These updates provided a near-real time opportunity to look at the response of surface water $CO_2$ to episodic events, such as passage of hurricanes, and yielded timely indications of instrument malfunction that could be remedied by company engineers on board or when the ships returned to port. The instruments have shown agreement to within 1 µatm with other state-of-art systems in intercomparison studies (Nojiri et al., Feb. 2009 pers. com.). Several different versions of the instrument have been deployed on the ships over the years but overall measurement principles and accuracies, estimated at better than 2 µatm (Pierrot et al., 2009; Wanninkhof et al., 2013), were maintained.

### 1.3.2 Thermosalinograph

Temperature and salinity were measured with a flow-through Seabird SBE45 thermosalinograph (TSG) that was in a seawater flow line parallel to the $pCO_2$ equilibrator. A SBE38 remote temperature probe was situated near the inlet before the pump, and was used as the SST measurement. The TSGs and temperature probes were maintained by collaborators from the Marine Technical group at the Rosenstiel School of Marine and Atmospheric Sciences at the University of Miami (RSMAS/U. Miami). The TSGs on the ships were factory calibrated on an annual basis. Post-calibrations showed no drift in the temperature sensor but occasionally some drift in the conductivity.

### 1.3.3 Other instrumentation

The underway effort is part of a larger scientific operation lead by RSMAS called Oceanscope (https://oceanscope.rsmas.miami.edu/). Additional instrumentation onboard the ships include the Marine-Atmospheric Emitted Radiance Interferometer (M-AERI) to assess surface skin temperature retrievals from a number of radiometers on earth-observation satellites (Minnet et al., 2001). The M-AERI's are Fourier-Transform Infrared interferometers situated on the deck viewing the sea surface away from the wake. Acoustic Doppler Current Profilers (ADCP) mounted on the hull of the ships are used to measure ocean currents.

## 2 Datasets

### 2.1 $pCO_2$ data

Full details on data acquisition with these systems and calculation of $pCO_2$ and $fCO_2$ can be found in Pierrot et al. (2009). Post-cruise, the $xCO_2$ data were processed by first linearly interpolating each standard measured every ~4 hours to the time of a sample measurement and then recalculating the air and water $xCO_2$ values based on the linear regression of the interpolated standard values at the time of sample measurement. For 3 cruises, the analyzer output showed negative water vapor values due to the condition of desiccant chemicals, and thus yielded erroneous dry $xCO_2$ values. Separate processing routines were developed to correct for these situations (available on request from D. Pierrot). The post-cruise corrected $xCO_2$ values were used for calculation of $pCO_2$ and $fCO_2$ as described in the calculation section.

### 2.2 Thermosalinograph, sea surface temperature and salinity data

The SST data were obtained from a temperature probe (Seabird, model SBE38) near the intake. The salinity was determined with a thermosalinograph (Seabird, model SBE45), from the measured conductivity and temperature in the unit using the internal software of the SBE45. The SST and SSS data were appended to the $pCO_2$ data records in real time and also logged via another shipboard computer at more frequent intervals. The SSS data was not quality controlled and no corrections to the

SSS data were made, other than removal of spikes and values that were out of range (<5 and > 40). As salinity has minimal effect on the calculated $fCO_2$, bad or missing salinities were removed and substituted by linearly interpolated values to eliminate gaps. When SST were not recorded in the $CO_2$ files, or in error, the SST gaps were filled from the high resolution SST data files maintained by the RSMAS Oceanscope project. On the rare occasion (≈<0.1 %) that SST was not recorded at all, SST data was estimated from the equilibrator temperature data ($T_{eq}$) after applying a constant offset between $T_{eq}$ and SST using SST data before and after the gap. On average the $T_{eq}$ was 0.12 ± 0.28˚C lower than SST for all the cruises. Per cruise the standard deviation (stdev) of the difference of $T_{eq}$ and SST was on the order of 0.04 ˚C. The in situ $pCO_2$ data calculated with $T_{eq}$ was flagged with a WOCE quality control flag of 3 which refers to data that is deemed questionable and has a larger uncertainty (https://www.nodc.noaa.gov/woce/woce_v3/wocedata_1/whp/exchange/exchange_format_desc.htm).

For the regionally mapped products on a 1-degree grid and monthly timescale (1˚ by 1˚ by mo), SST and SSS were obtained from the following sources: The SSS data were from a numerical model, the Hybrid Coordinate Ocean Model (HYCOM) (https://HYCOM.org/) and referred to as $SSS_{HYCOM}$. The SST product for the region is the Optimum Interpolated SST, OISST from https://www.esrl.noaa.gov/psd/., (Reynolds et al., 2007). It uses data from ships, buoys and satellites to generate the fields. For the OISST the reference SST is from buoys, and the other SST data obtained from ships and other platforms were adjusted to the buoy data by subtracting 0.14˚C in the OISST product (Reynolds et al., 2007).

### 2.3 Wind speed data

Winds were measured on the ships but these data are not used as they are not synoptic for the whole region which is a requirement for the regional flux maps. Instead, wind speeds were obtained from the updated cross-calibrated multi-platform wind product (CCMP-2) (Atlas et al., 2011). The mean scalar neutral wind at 10 m height $\langle u_{10} \rangle$, and its second moment $\langle u_{10}^2 \rangle$ were used to calculate the fluxes. They were determined from the ¼ degree, 6-hourly product that was obtained from Remote Sensing Systems (RSS) (www.remss.com). This product relies heavily on the European Center for Median Weather Forecasting (ECMWF) assimilation scheme that uses in situ and remotely sensed assets, particularly (passive) radiometers on satellites. The directional component uses scatterometer data. The ¼ degree, 6-hourly CCMP-2 product was binned and averaged in 1-degree grid boxes on monthly scales (1˚ by 1˚ by mo). In absence of CCMP-2 data for 2018, the wind product from European Reanalysis, ERA5, was used (https://www.ecmwf.int/en/forecasts/datasets/reanalysis-datasets/era5, Copernicus Climate Change Service, 2017). The ERA5 wind data are at 31-km and 3-hourly resolution but were binned and averaged in the same manner as the CCMP-2 winds. There were no apparent biases between the scalar winds for the two products in the Caribbean.

### 2.4 Mixed layer depth data

No MLD determinations were made on the cruises and limited observational estimates from other sources are available. The MLDs provided here are from the same numerical model (HYCOM) as used for the mapped SSS, and obtained from http://www.science.oregonstate.edu/ocean.productivity/index.php. The MLDs are based on a density contrast of 0.03 between

surface and subsurface. Mixed layer depths (MLD) are used as an independent variable in the MLRs to map the $fCO_{2w}$ values. They are also needed if mixed layer dissolved inorganic carbon (DIC) inventories are desired, and to determine the effect of mixed layer depth on the changes in $fCO_{2w}$. As shown in Wanninkhof (2019b, Figure 9), MLDs are negatively correlated with $fCO_{2w}$. They are provided in the gridded mapped product.

## 3 Calculations

The calculations of the concentrations and fluxes follow standard procedures as described below. The mapping procedures are detailed. The section on uncertainty includes an example of different possible means of mapping and the effect on the final product.

### 3.1 Calculation of $pCO_2$

The starting point in the calculations, which were aided by use of MATLAB routines following the procedures as in Pierrot et al. (2009), were calibrated (dry) $xCO_2$ values.

The $xCO_2$ values were converted to $pCO_{2eq}$ (µatm) values:

$$pCO_{2eq} = xCO_{2eq} (P_{eq}\text{-}pH_2O) \quad (1)$$

where eq refers to equilibrator conditions. The $P_{eq}$ is the pressure in the equilibrator headspace and $pH_2O$ is the water vapor pressure calculated according to Eq. 10 in Weiss and Price (1980). The $pCO_{2eq}$ was corrected to surface water values using the intake temperature (SST) and the temperature of water in the equilibrator ($T_{eq}$) according to the empirical relationship that Takahashi et al. (1993) developed for North Atlantic surface waters:

$$pCO_{2w} = pCO_{2eq}\, e^{(0.0423(SST-Teq))} \quad (2)$$

This empirical correction for temperature is widely used but it is of note that applying the thermodynamic relationships for carbonate dissociation constants yields different temperature dependencies that are a function of temperature. For average SST in the Caribbean of 27.0 ˚C the coefficient of temperature dependence varies from 0.036 to 0.040 using commonly used constants as provided in inorganic carbon system programs such as CO2SYS (Pierrot et al, 2006) compared to the coefficient of 0.0423 (or 4.23 % $˚C^{-1}$) used above. On average the difference between SST and $T_{eq}$ is 0.12 ˚C for all the cruises such that the correction from $T_{eq}$ to SST using the coefficient of 0.0423 in Eq. 2 is 1.9 µatm under average conditions of SST= 27 ˚C and $pCO_{2w}$ =374 µatm. Using a temperature coefficient of 0.036 the temperature correction would be 1.6 µatm, or a 0.3 µatm difference.

### 3.2 Calculation of $fCO_2$ in air and water

The $fCO_2$ is the $pCO_2$ corrected for non-ideality of $CO_2$ solubility in water using the virial equation of state (Weiss, 1974). The correction can be expressed as: $fCO_{2a,w} = e^{g(SST,P)}\, pCO_{2a,w}$

and:

$$g(T,P)=[(-1636.75+12.0408T-0.0327957T^2+0.0000316528T^3)+2(1-xCO_2\,10^{-6})^2\,(57.7-0.118T)$$
$$(P/1013.25)]/(82.0575T) \quad (3)$$

where T is in Kelvin, $xCO_2$ is in ppm, and P is in mbar.

Under average conditions in the Caribbean, the function $e^{g(SST,P)} \approx 0.997$ and $fCO_{2w}$ will be ≈ 1.2 µatm less than $pCO_{2w}$. As the corrections from partial pressure to fugacity in air and water are approximately the same, the difference between $\Delta pCO_2$ ($=pCO_{2w}-pCO_{2a}$) and $\Delta fCO_2$ ($=fCO_{2w}-fCO_{2a}$), that were used to determine the fluxes (Eq. 5), is negligible (≈<0.1 µatm).

### 3.3 Gridding procedure

Gridding of the observations of $fCO_{2w}$, SST, and SSS was performed by binning and averaging the data in (1˚ by 1˚ by mo) cells. At typical ship speeds of 22 knots, the ship covered 1˚ in about 2.5 hours taking 60 measurements. This would yield about 250 measurements per month assuming weekly cruises through the area. The actual number of measurements per grid cell ranged from 8 to 500. The higher number of observations per cell were mostly in the latter part of the record, when the *Eqnx* and *ALoS* operated in the same area. The total number of observations from March 2002 through December 2018 was 1.13 million, and the total number of (1˚ by 1˚ by mo) grid cells with observations was 9224.

The gridding facilitated the co-location and merging of products such as $MLD_{HYCOM}$, $SSS_{HYCOM}$, OISST, $\langle u^2 \rangle_{CCMP}$, and Marine Boundary Layer (MBL) $xCO_2$, $xCO_{2aMBL}$, into the gridded observational dataset for further interpretation. The gridded data aided comparison of *in situ* SST with OISST and SSS with $SSS_{HYCOM}$. The average difference between SSS and $SSS_{HYCOM}$ for the 2002-2018 data was -0.1 ± 0.28 (n= 9224), and for SST and OISST the difference was 0.25 ± 0.40 ˚C (n= 9224) with the in situ SSS being lower and SST being higher. While both differences include zero within their standard deviation, the temperature difference is in agreement with expected cooler near-surface temperatures that could lead to lower $fCO_{2w}$ which, in turn, have a large impact on the calculated air-sea fluxes.

### 3.4 Mapping procedures for $fCO_{2w}$ and fluxes

#### 3.4.1 Mapping $fCO_{2w}$ using a multi-linear regression

The gridded observations (1˚ by 1˚ by mo) represented about 10 % of the area and months of investigation from 15 to 28 ˚N and 88 to 62 ˚W over the period of investigation. To interpolate ("map") the data in space (334 grid cells) and time (192 months) a multi-linear regression (MLR) approach was used to determine $fCO_{2w}$ in each grid cell. For each year from 2002 through 2018 the gridded $fCO_{2w}$ observations were regressed against the 1-degree monthly gridded values of position (Lat and Lon), SST, MLD, and SSS. Other permutations of independent parameters were tested but yielded less robust fits (see Appendix A). Annual MLRs were created as $fCO_{2w}$ levels change over time in response to increasing atmospheric $CO_2$ levels. If $fCO_{2w}$ kept pace with atmospheric $CO_2$ increase this would translate to a linear trend of $fCO_{2w}$ of 2.13 µatm $yr^{-1}$ over the time period. As shown in Wanninkhof et al. (2019b), multi-year (>4-yr intervals) trends varied from -4 to 4 µatm $yr^{-1}$, with an average linear trend in $fCO_{2w}$ of 1.4 µatm $yr^{-1}$ from 2002-2018.

The annual MLRs were created of the form:

$$fCO_{2w} = a\ Lon + b\ Lat + c\ OISST + d\ MLD_{Hycom} + e\ SSS_{Hycom} + f \quad (4)$$

with the coefficients for each year, along with the standard error in $fCO_{2w}$ and standard error in each of the coefficients provided in Table 1. The standard error in the $fCO_{2wMLR}$ ranged from 5 to 9 µatm for each year. Using the locations, OISST (the optimal interpolated SST product), $MLD_{Hycom}$ and the $SSS_{Hycom}$ (output of the HYCOM model) the $fCO_{2MLR}$ is determined for each grid cell. There were significant cross-correlations between independent variables such that the effect of the often significant year-to-year differences in coefficients was difficult to interpret. However, the $fCO_{2wMLR}$ from the annual MLRs faithfully reproduced the trends and variability.

The MLRs were produced for each year such that the mapped products could be extended for future years in a straightforward fashion. To determine if there were anomalous discontinuities between subsequent annual MLRs that could impact the timeseries, the difference between $fCO_{2w}$ for subsequent months were plotted versus time in Figure 3. No significant discontinuities were observed between December and January. Only for December and January 2008/2009, 2009/2010, and 2016/2017 there appear to be slight differences in the pattern of monthly progressions but such anomalies are observed during other times of year as well. Using an MLR that includes year as one of the coefficients (see, Appendix A, Eqs. A3 and A4) provides a slightly worse fit. Moreover, using such a fit would necessitate recalculating the mapped products every time a new year is added.

As illustration of differences between gridded and mapped products the results of the $fCO_{2wMLR}$ calculated with the MLRs for 2004, 2011, and 2017 (Table 1) are plotted in Figure 4a along with the gridded observations for the grid cells that span the longitude range from 88˚W to 62˚ W between 23˚ N and 24˚ N (see Fig.1). Figure 4a shows that the mapped product using annual MLRs show the increases in $fCO_{2w}$ over time in the region, and consistent differences in patterns between the East and the West for the three years. The mapped product showed a reasonable correspondence with the gridded observations. Some of the differences between the gridded observations and mapped product were caused by the mismatch between SST and SSS *in situ* with the OISST and $SSS_{HYCOM}$ (Figs. 4b and 4c). In particular, the strong minima in OISST at 79˚ W is not seen in the SST. This is likely because the OISST captured the lower SST near the coast of Cuba. This caused the $fCO_{2wMLR}$ product to be lower as well, as shown in Figure 4a. It illustrates that the mapped $fCO_{2wMLR}$ product is both influenced by the annual MLR, and the gridded $MLD_{Hycom}$, OISST, and $SSS_{Hycom}$.

### 3.4.2 Determining the air-sea $CO_2$ fluxes for the region

For the determination of the air-sea $CO_2$ flux ($F_{CO2}$, mol $m^{-2}$ $yr^{-1}$), a bulk formulation was applied using the gridded mapped product:

$$F_{CO2} = k\ K_0\ \Delta fCO_2 \quad (5)$$

where $\Delta fCO_2$ is ($fCO_{2w}$-$fCO_{2a}$), $K_0$ is the seawater $CO_2$ solubility that is a function of temperature and salinity (Weiss and Price, 1980), and k is the gas transfer velocity parameterized as a function of wind speed (Wanninkhof, 2014):

$$k = 0.251 <u_{10}^2> (Sc/660)^{-1/2} \quad (6)$$

where $<u_{10}^2>$ is the monthly 2nd moment of the wind speeds reported in CCMP-2. The 2nd moment accounts for the impact of variability of the wind speed on k. It is determined by taking the monthly average of the sum of squares of the wind speed in CCMP-2 provided at 6-hours and ¼˚ grid resolution. The number of wind speed observation in a (1˚ by 1˚ by mo) grid is 1920. This sample density captures the frequency spectrum of winds in the grid boxes except that extreme wind events such as hurricanes are not fully represented due to the local nature of the extremes and inherent smoothing in the CCMP-2 product. The Sc is the Schmidt number of $CO_2$ in seawater, defined as the kinematic viscosity of seawater divided by the molecular diffusion coefficient of $CO_2$. It is determined as a function of temperature from Wanninkhof (2014). At the average temperature of 27 ˚C the $Sc_{CO2}$ equals 475. Over the typical range of SST in the Caribbean from 24 ˚C to 30 ˚C, the $(Sc/660)^{-1/2}$ will vary from 1.1 to 1.27, indicating that the gas transfer velocity will be 27 % higher at an SST of 30 ˚C compared to a SST of 20 ˚C that would correspond to a Sc of 660.

The annual $fCO_{2MLR}$, and modeled and remote sensed products, OISST, $MLD_{HYCOM}$, $SSS_{HYCOM}$, were determined for all (1˚ by 1˚ by mo) grid cells. The monthly $fCO_{2aMBL}$ values were derived from the weekly average $xCO_{2aMBL}$ of the stations on Key Biscayne (KEY) and Ragged Point Barbados (RPB) (CarbonTracker Team, 2019; https://www.esrl.noaa.gov/gmd/ccgg/flask.php). The second moments of the scalar winds, $<u^2>$ from CCMP-2 were averaged on the same grids. As no CCMP-2 product was available in 2018, the ERA5 wind product was used for the last year of the record.

**Table 1**. Coefficients for the MLR for each year*

### 3.5 Gridded and mapped products for Alkalinity and $pH_T$

Total Alkalinity (TA) was determined from salinity. For estimation of TA, several algorithms have been developed with salinity (Fig. 5 ) (Millero et al., 1998; Lee et al., 2006; Takahashi et al., 2014 and Cai et al., 2010). The relationship of Cai et al. (2010), TA= 57.3 SSS+ 296.4, stdev = 5.5 was used as this was determined from observations that are similar to the conditions in the Caribbean.

The $pH_T$, the pH on the Total scale at SST, was subsequently determined from the calculated TA and $fCO_{2w}$. For the gridded products the gridded SSS was used to determined TA. For the $pH_T$ the gridded TA, SST and $fCO_{2w}$. were used. For the mapped products the gridded OISST and $SSS_{Hycom}$ were applied in the calculations. The $pH_T$ was calculated using the program CO2SYS for Excel V2.2 (Pierrot et al., 2006) with the apparent $CO_2$ dissociation constants, $K_1$, $K_2$ from Lueker et al. (2000); the $KSO_4^-$ dissociation constant from Dickson (1990); the KF dissociation constant from Perez and Fraga (1987); and the total boron relationship with salinity from Uppström (1974).

### 3.6 Aragonite saturation state ($\Omega_{Ar}$)

The aragonite saturation state ($\Omega_{Ar}$) indicates the level of supersaturation or undersaturation of seawater with respect to the mineral aragonite, a polymorph of calcium carbonate, and part of the skeletal structure of many marine calcifiers. When $\Omega_{Ar}$ is less than 1 aragonite dissolution is thermodynamically favored and when $\Omega_{Ar}$ is greater than 1, it has a tendency to precipitate. The $\Omega_{Ar}$ is used as an indicator of ecosystem health with regards to ocean acidification (Mollica et al., 2018). In warm tropical regions surface water saturation states are well above one but no active precipitation takes place except under unusual circumstances in shallow waters, in a precipitation process called whitings (Purkis et al., 2017). The $\Omega_{Ar}$ is not measured directly and is defined as the product of calcium and carbonate ion concentrations divided by the solubility product of aragonite:

$$\Omega_{Ar} = [Ca^{2+}]\,[CO_3^{2-}]\,(K_{Ar}'_{sp})^{-1} \quad (7)$$

where $[Ca^{2+}]$ is the total calcium concentration and is derived from salinity: $[Ca^{2+}] = 0.02128 / 40.087 * (SSS/ 1.80655) = 293.84$ S in mol/kg-SW (Riley and Tongudai, 1967). $[CO_3^{2-}]$ is the total carbonate ion concentration determined from two of the inorganic carbon system parameters, and $K_{Ar}'_{sp}$ is the apparent solubility product of aragonite in seawater at a specified salinity, temperature and pressure. In this work $[CO_3^{2-}]$ was determined from the gridded $fCO_{2w}$ and calculated TA using the CO2SYS program. For surface waters, $K_{Ar}'_{sp}$ is

$$pK_{Ar}'_{sp} = -[-171.945 - 0.077993\,T + 2903.293/T + 71.595\log(T) + (-0.068393 + 0.0017276\,T + 88.135/T)\,S^{0.5} - 0.10018\,S + 0.0059415\,S^{1.5}] \quad (8)$$

where $pK_{Ar}'_{sp} = -\log K_{Ar}'_{sp}$, T is temperature in Kelvin (K), and S is salinity (Mucci,1983). As with $pH_T$, the $\Omega_{Ar}$ gridded product was determined from the gridded (1˚ by 1˚ by mo) values of SSS, SST, $fCO_{2w}$ and TA, while the mapped product uses $SSS_{Hycom}$, OISST, $fCO_{2wMLR}$ and TA.

### 3.7 Uncertainty of observations, gridded and mapped products

The uncertainty of the products is difficult to quantify due to the many factors, calculations, and interpolations influencing the overall uncertainty. Moreover, the uncertainty estimate includes a random and a systematic component. The latter can have a large influence on interpretations, particularly on the calculated air-sea $CO_2$ fluxes. Below we address the uncertainty in terms of standard errors in the observations; in the gridded products; and in the mapped products. For the calculated quantities and nomenclature we follow the approach in Orr et al. (2018). The standard uncertainty is characterized by its standard deviation/error of the measured quantities and the standard uncertainties of the input variables. The propagated uncertainty of

a calculated variable is called the combined standard uncertainty. Error propagation for addition is $(e_A^2 + e_B^2 + \ldots..)^{0.5}$ and for multiplication it is $((e_A/A)^2 + (e_B/B)^2 + \ldots.)^{0.5}$, where A and B are the variables, and $e_A$ is the standard error in variable A.

The individual measurements of $fCO_{2w}$ have a combined standard uncertainty of less than 2 µatm based on a propagation of error of instrument response, equilibrator efficiency standardization, and temperatures and pressures at equilibration and at the sea surface (Pierrot et al., 2006). The performance and output data from the $UWpCO_2$ systems have been checked at manufacturer, in intercomparison exercises, and at sea. SST measurements, at point of measurement, are accurate to 0.02 ˚C and SSS to 0.1 based on instrument specifications and annual calibrations.

The combined standard uncertainty in gridded product will vary based on the number of measurements. It includes the actual variability in the 1˚ by 1˚ cells. To estimate the uncertainty per grid cell, the standard deviation of the $fCO_{2w}$ in each cell was determined and then the average of the standard deviations for the 9924 cells with observations was taken. The average standard deviation was 3.4 ± 2.6 µatm (n=9224). The same procedure was followed for SST and SSS and yielded values of 0.22± 0.19 ˚C for SST; and 0.10± 0.10 for SSS. These were relatively small uncertainties compared to the monthly spatial range of ≈ 20 µatm for $fCO_{2w}$; ≈1 ˚C for SST; ≈1 in SSS. The amplitude of the seasonal cycle of ≈40 µatm for $fCO_{2w}$ and ≈4 ˚C for SST were significantly greater than the standard uncertainties as well.

The calculated parameters for the gridded products, TA, $pH_T$ and $\Omega_{Ar}$ have an added uncertainty due to the uncertainty in the constants and parameterizations. The agreement between TA-SSS relationships was good, and choice of TA relationship did not have a determining influence on results. We used TA=57.3 SSS_OBS + 296.4 specifically developed for the Subtropical Western Atlantic (see insert of Figure 10 in Cai et al., 2010). The standard error for the relationship was 5.5 µmol $kg^{-1}$. The average standard deviation for salinity in the grid cells is 0.1 which translates to an uncertainty gridded TA of 5.7 µmol $kg^{-1}$. Thus the combined standard uncertainty for TA is $((5.5)^2+(5.7)^2)^{0.5} = 7.9$ µmol $kg^{-1}$.

$pH_T$ is determined from $fCO_{2w}$ and calculated TA with associated uncertainties. An added uncertainty for the calculated $pH_T$ is the uncertainty in the dissociation constants that are used to calculate $pH_T$ . These uncertainties can be calculated using a modified version of CO2SYS (Orr et al. 2018). As shown in Orr et al. (2018, Figure12), the uncertainty in the constants dominates the calculated $pH_T$. Using the uncertainty in the constants as presented in the program, an uncertainty of gridded TA of 8 µmol $kg^{-1}$ and 3.4 µatm for $fCO_2$ yields a combined standard uncertainty in pH of 0.0075. For comparison the uncertainty in pH would be 0.0070 if state-of-the art measurement uncertainties in TA of ±3 µmol $kg^{-1}$ and ±2 µatm for $fCO_2$ are used. Similarly, the uncertainty $\Omega_{Ar}$ using the same approach and uncertainties in independent parameters is ±0.20. Again it is the uncertainty in the dissociation constants that dominate the overall uncertainty.

For the mapped products there is the additional uncertainty due to the use of regressions. The standard errors of the annual regressions in $fCO_{2wMLR}$ and the coefficients of the independent parameters are provided in Table 1. The average standard error for the $fCO_{2wMLR}$ for the 17 years is 6.4 ± 1.2 µatm. Following the approach above for the other independent parameters and propagating these uncertainties yields a combined standard uncertainty of 0.0090 in mapped pH and 0.21 in mapped $\Omega_{Ar}$

Systematic errors are introduced by the different SST and SSS data that are used for the gridded and mapped products, with the former using the gridded measured SST and SSS, and the latter using the $SSS_{Hycom}$ and OISST products. The magnitude of the systematic uncertainty between the mapped and gridded product is estimated from the difference in the gridded and mapped parameters for cells that have both gridded and mapped products (for columns headers, see Table 2). Another possible source of systematic uncertainty is using the gridded and mapped $fCO_{2sw}$, SSS, and SST to calculate the TA, $pH_T$ and $\Omega_{Ar}$ rather than using the in situ values to calculate the parameters and then gridding them. This uncertainty is small based on the low uncertainty of variables in each cell as shown from their standard deviations provided in the gridded products (for column headers, see Table 3).

This is confirmed by comparing this method with the approach of calculating the pH and then gridding and mapping as done in Lauvset et al. (2016) and Jiang et al. (2015). To examine the differences derived from using one or the other approach, both were compared for 2017 data. The pH and TA were calculated for every $fCO_{2w}$ observation and binned into a (1˚ x 1˚ x mo) grid. A MLR from the calculated pH was created for 2017:

$$pH_T(\pm 0.005) = 0.0003194\ Lon - 0.00046744\ Lat - 0.00965183\ SST + 0.00019602\ MLD + 0.00069378\ SSS + 8.3240 \qquad r^2 = 0.89\ (n = 1244) \qquad (9)$$

This MLR was then applied to the independent variables for each grid box to determine $pH_T(MLR)$. This was compared to the approach used here of calculating the pH using the mapped $fCO_{2wMLR}$ and TA-SSS relationships on (1˚ x 1˚ x mo) grids, called $pH_T(fCO_{2w},TA)$. The two approaches provided similar results with $pH_T(fCO_{2w},TA) - pH_T(MLR) = -0.0001 \pm 0.005$ for 2017. The small difference showed a pattern with SST (Fig. 6) but not with the other independent variables. The differences using either $pH_T(fCO_{2w},TA)$ or $pH_{T,MLR}$ are an order of magnitude smaller than the combined standard uncertainties such that the approach of using mapped $fCO_{2w}$ and TA to determine $pH_T(MLR)$ yielded precise and consistent gridded $pH_T$.

Calculated air-sea $CO_2$ fluxes have a significant uncertainty as they are driven by relatively small air-water concentration differences. Using the uncertainty in $fCO_{2wMLR}$ of 6.4 µatm and an uncertainty $fCO_{2a}$ of 1 µatm, and uncertainties in k of 20 % (Wanninkhof, 2014) and $K_0$ of 0.002 (Weiss, 1974), the corresponding combined standard uncertainty is 21 % for the flux. For flux calculations the systematic error, or bias, is a big issue. The near-surface temperature gradient and skin temperatures will have an impact on the $fCO_{2w}$ and $K_0$. The magnitude, along with its applicability to the bulk flux formulation is under debate (McGillis and Wanninkhof, 2006; Woolf et al., 2016). For the mapped product, the OISST is used. The OISST uses a variety of temperature data, including remote sensing of the skin temperature and the product is adjusted to buoy temperatures nominally at 1-m (Reynolds et al., 2007) such that implicitly a common reference depth is used for $fCO_{2wMLR}$. As shown in Wanninkhof et al. (2019b) the OISST was on average 0.25 ˚C lower than SST, and using the SST instead of the OISST would change the flux from -0.87 to -0.63 mol $m^{-2}$ $yr^{-1}$ a 27 % decrease. If OISST is used for bulk temperature and using a canonical value for difference in bulk and skin temperature of 0.17 ˚C, it would increase the uptake of $CO_2$ by 18 % from -0.87 to -1.04 mol $m^{-2}$ $yr^{-1}$. Based on current knowledge, we believe that using the OISST and the resulting calculated $fCO_{2wMLR}$ as was done here yields the appropriate fluxes.

**Table 2.** Estimated uncertainties in measured, gridded, and mapped variables

## 4 Datasets and data products

Several different data products are provided in conjunction with this paper. The methodology to create the products is described above, and here the file format and column headers is presented with a brief description when warranted.

### 4.1 Underway $pCO_2$ data

The quality controlled cruise data are posted at different locations. The individual cruise files with metadata can be found at https://www.aoml.noaa.gov/ocd/ocdweb/occ.html. Data can be found as part of the SOCAT holdings (Bakker et al. 2016) using an interactive graphical user interface https://ferret.pmel.noaa.gov/socat/las/. In addition, cruise files of the three ships are provided in annual directories at the National Center for Environmental Information (NCEI) (https://www.nodc.noaa.gov/ocads/oceans/VOS_Program/explorer.html). The data file structures are from the MATLAB data reduction program of Pierrot (pers. comm.).The primary identifier for the cruises is the EXPO code which is the International Council for the Exploration of the Sea (ICES) ship code and the day the ship starts the cruise. Examples are as follows: For a cruise of the *EoS* starting March 6, 2002, the EXPO code is 33KF20020306; for an *ALoS* cruise starting November 25, 2018, the EXPO code is BHAF20181125, and for the *Eqnx* cruise departing her homeport on February 10, 2018, it is MLCE20180210. The individual cruise files at the sites above sometimes include data outside the study region.

### 4.2 Gridded data

The gridded datasets are the binned and averaged $fCO_{2w}$, SST, and SSS observations on a (1˚ by 1˚ by mo) grid. The files include the auxiliary data obtained from remote sensing and interpolated data (OISST), data assimilation of remotely sensed winds (CCMP-2) ,and from the HYCOM model ($SSS_{HYCOM}$). Calculated TA, $pH_T$ and $\Omega_{Ar}$ using procedures outlined above are provided in the file. The calculated $fCO_{2w}$ using the annual MLRs (Table 1) are provided as well. This gridded data set has spatial and temporal gaps as the ships did not transit through each pixel, and coverage is uneven. The number of observations differ for each grid cell and are listed in the gridded data set. For the auxiliary data the number of data points are fixed by the resolution of the data products except where part of the grid includes land which is masked. The column headers are provided in Table 3 and include units and descriptions when warranted.

**Table 3.** Column headers for the monthly 1-degree gridded observational product (1˚ by 1˚ by mo)

### 4.3 Mapped product

The mapped product provides the data on a homogeneous (1˚ by 1˚ by mo) grid boxes utilizing the annual MLRs of $fCO_{2w}$ as a function of Lat, Lon, OISST, $SSS_{HYCOM}$, and $MLD_{HYCOM}$ for the region from 15˚ N to 28˚ N and -62˚ to -88˚ (= 62˚ W to 88˚ W). The modeled and remotely sensed products OISST, $SSS_{HYCOM}$, and $MLD_{HYCOM}$ and position were used in the MLR (Eq. 4) as the independent parameters. The mapped product includes the air-sea $CO_2$ fluxes in the region as a specific flux (mol $m^{-2}$ $yr^{-1}$) for each grid box. The column headers are provided in Table 4 including units and descriptions when warranted.

**Table 4.** Column headers for the monthly 1-degree mapped product (1˚ by 1˚ by mo) for the whole region

### 4.4 Monthly and Annual estimates for the Caribbean 2002-2018

Summary files of monthly and annual data and products covering the whole region from 15º N to 28˚ N and 88º W and 62˚ W are provided based on averaging or summing the data in the mapped products. The column headers for the monthly and annual products are similar (Tables 5 and 6). For the monthly files the average of each parameter for each cell are area weighted based on the area of the cell as provided in the mapped product (Table 4) according to: area cell/(total area/#of cells). The total $CO_2$ mass flux ($CO_2_Flux_{Total}$) is the integral of the monthly area weighted $CO_2$ fluxes (mol $m^{-2}$ $yr^{-1}$) expressed in teragrams of carbon (= $10^{12}$ g C) per month or per year.

**Table 5.** Column headers for the monthly averaged mapped product

**Table 6.** Column headers for the annual averaged mapped product

## 5 Data availability

The observations are available at three locations in slightly different formats but all files are stored by ship and cruise. The primary source is the website at the Atlantic Oceanographic and Meteorological Laboratory (AOML) (https://www.aoml.noaa.gov/ocd/ocdweb/occ.html). These data are submitted to SOCAT at least once a year such that they can be posted in the annual updates of SOCAT (https://socat.info). The permanent depository of the data is at NCEI where the data are stored per cruise in directories listed per year (https://www.nodc.noaa.gov/ocads/oceans/VOS_Program/explorer.html). The gridded observations and mapped products described herein are posted at directories at AOML and NCEI. The dataset, and derived quantities are provided on a 1-degree monthly grid at http://accession.nodc.noaa.gov/0207749, https://doi.org/10.25921/2swk-9w56 (Wanninkhof et al., 2019a). The products cover the years 2002 through 2018 and will be updated annually.

## 6 Conclusions

The datasets from the cruise ships sailing the Caribbean Sea are a rich resource for studying the trends and patterns of inorganic carbon cycling and ocean acidification in the region. The scales of variability and data density are such that the (1˚ by 1˚ by mo) monthly gridding captures the magnitudes and trends of $fCO_{2w}$ and derived inorganic carbon products on seasonal to interannual scales. Using annual MLRs to interpolate $fCO_{2w}$ with position, SST, SSS, and MLD as independent variables yielded accurate monthly products (Wanninkhof et al., 2019a). A comprehensive investigation of the changes in decadal trends based on the dataset and products was presented in Wanninkhof et al. (2019b). The combined standard uncertainties and systematic offsets of gridding and mapping were estimated from comparing $fCO_{2w}$ observations with gridded and mapped products including TA, $pH_T$ and $\Omega_{Ar}$. The MLRs capture the spatial and temporal variability in $fCO_{2w}$ and calculated $pH_T$ and $\Omega_{Ar}$ well in the region. The datasets and products are invaluable for model initiation and validation, and serve as boundary conditions for near-shore fine scale models.


## Team list

This work was done on Royal Caribbean Cruise Lines (RCCL) ships who provided access, and personnel and infrastructure resources for the measurement campaign coordinated through the Rosenstiel School of Marine and Atmospheric Sciences (RSMAS) of the University of Miami (U. Miami). Peter Ortner, Elizabeth Williams, Don Cucchiara and Chip Maxwell of the Marine Technical group at RSMAS/U. Miami have been instrumental in maintaining the science operations. Denis Pierrot, Kevin Sullivan, Leticia Barbero, Robert Castle (ret.), and Betty Huss of NOAA/AOML have led the gathering, maintenance, data processing and posting of $fCO_2$ data. In addition to $fCO_2$ measurements; skin temperature (MAERI), led by P. Minnet and M. Izaguirre, RSMAS; TSG with instruments, supplied by G. Goni and F. Bringas of AOML; optics; and ADCP, with data processed at the University of Hawaii Currents center (E. Firing and J. Hummon), operations take place on the RCCL ships.


## Author contributions

All authors contributed to writing and editing the documents. JT performed most of the gridding and binning, and provided the model and remotely sensed data from the sources listed in the text. KF and DP performed maintenance and data reduction, and liaised with all parties involved in the operations.

## Competing interests

The authors of this manuscript have no competing interest involving this work.

**Acknowledgments**

This work would not have been possible without support from Royal Caribbean Cruise Lines who have provided access to their ships and significant financial, personnel, and infrastructure resources for the measurement campaign coordinated through the Rosenstiel School of Marine and Atmospheric Sciences of the University of Miami. David Munro INSTAR, ESRL/GMD provided the KEY and RPB $CO_2$ data. NOAA Optimal Interpolated SST data were provided by the NOAA/OAR/ESRL/PSD. The NOAA office of Oceanic and Atmospheric Research (OAR) is acknowledged for financial support, in particular the Ocean Observations and Monitoring Division (OOMD) (fund reference 100007298), and the NOAA/OAR Ocean Acidification Program.

**References**

Atlas, R., Hoffman, R. N., Ardizzone, J., Leidner, S. M., Jusem, J. C., Smith, D. K., and Gombos, D.: A cross-calibrated multiplatform ocean surface wind velocity product for meteorological and oceanographic applications, Bull. Amer. Meteor. Soc., 92, 157-174, https://doi.org/10.1175/2010BAMA2946.1, 2011.

Bakker, D. C. E., Pfeil, B., Landa, C. S., Metzl, N., O'Brien, K. M., Olsen, A., Smith, K., Cosca, C., Harasawa, S., Jones, S. D., Nakaoka, S. I., Nojiri, Y., Schuster, U., Steinhoff, T., Sweeney, C., Takahashi, T., Tilbrook, B., Wada, C., Wanninkhof, R., Alin, S. R., Balestrini, C. F., Barbero, L., Bates, N. R., Bianchi, A. A., Bonou, F., Boutin, J., Bozec, Y., Burger, E. F., Cai, W. J., Castle, R. D., Chen, L., Chierici, M., Currie, K., Evans, W., Featherstone, C., Feely, R. A., Fransson, A., Goyet, C., Greenwood, N., Gregor, L., Hankin, S., Hardman-Mountford, N. J., Harlay, J., Hauck, J., Hoppema, M., Humphreys, M. P., Hunt, C. W., Huss, B., Ibánhez, J. S. P., Johannessen, T., Keeling, R., Kitidis, V., Körtzinger, A., Kozyr, A., Krasakopoulou, E., Kuwata, A., Landschützer, P., Lauvset, S. K., Lefèvre, N., Lo Monaco, C., Manke, A., Mathis, J. T., Merlivat, L., Millero, F. J., Monteiro, P. M. S., Munro, D. R., Murata, A., Newberger, T., Omar, A. M., Ono, T., Paterson, K., Pearce, D., Pierrot, D., Robbins, L. L., Saito, S., Salisbury, J., Schlitzer, R., Schneider, B., Schweitzer, R., Sieger, R., Skjelvan, I., Sullivan, K. F., Sutherland, S. C., Sutton, A. J., Tadokoro, K., Telszewski, M., Tuma, M., Van Heuven, S. M. A. C., Vandemark, D., Ward, B., Watson, A. J., and Xu, S.: A multi-decade record of high-quality $fCO_2$ data in version 3 of the Surface Ocean CO2 Atlas (SOCAT), Earth Syst. Sci. Data 8, 383-413, https://doi.org/10.5194/essd-8-383-2016, 2016.

Boutin, J., Merlivat, L., Henocq, C., Martin, N., and Sallee, J. B.: Air–sea $CO_2$ flux variability in frontal regions of the Southern Ocean from CARbon Interface OCean Atmosphere drifters, Limnol and Oceanogr., 53, 2062-2079, 2008.

Cai, W.-J., Hu, X., Huang, W.-J., Wang, Y., Peng, T.-H., and Zhang, X.: Alkalinity distribution in the Western North Atlantic Ocean margins, J Geophys. Res., 115, https://doi.org/10.1029/2009JC005482, 2010.

Copernicus Climate Change Service (C3S) (2017): ERA5: Fifth generation of ECMWF atmospheric reanalyses of the global climate. Copernicus Climate Change Service Climate Data Store (CDS), *date of access July 9, 2019*. https://cds.climate.copernicus.eu/cdsapp#!/home

CarbonTracker Team Compilation of near real time atmospheric carbon dioxide data; obspack_co2_1_NRT_v4.4.2_2019-06-10; NOAA Earth System Research Laboratory, Global Monitoring Division. http://doi.org/10.25925/20190610, 2019.

DeGrandpre, M. D., Olbu, G. J., Beatty, C. M., and Hammar, T. R.: Air–sea $CO_2$ fluxes on the US Middle Atlantic Bight, Deep Sea Research Part II: Topical Studies in Oceanography, 49, 4355-4367, 2002.

Dickson, A. G.: Standard potential of the reaction: AgCl(s) + 1/2 $H_2$(g) = Ag(s) + HCl(aq), and the standard acidity constant of the ion $HSO_4^-$ in synthetic seawater from 273.15 to 318.15 K, Journal of Chemical Thermodynamics 22, 113-127, 1990.

Evans, W., Mathis, J. T., Cross, J. N., Bates, N. R., Frey, K. E., Else, B. G. T., Papkyriakou, T. N., DeGrandpre, M. D., Islam, F., Cai, W.-J., Chen, B., Yamamoto-Kawai, M., Carmack, E., Williams, W. J., and Takahashi, T.: Sea-air $CO_2$ exchange in the western Arctic coastal ocean, Global Biogeochemical Cycles, 2015GB005153, https://doi.org/10.1002/2015gb005153, 2015.

Gledhill, D. K., Wanninkhof, R., Millero, F. J., and Eakin, M.: Ocean acidification of the greater Caribbean region 1996-2006, J Geophys. Res., 113, C10031, https://doi.org/10.1029/2007JC004629, 2008.

Gomez, F. A., Wanninkhof, R., Barbero, L., Lee, S. K., and Hernandez Jr, F. J.: Seasonal patterns of surface inorganic carbon system variables in the Gulf of Mexico inferred from a regional high-resolution ocean biogeochemical model, Biogeosciences, 17, 1685-1700, https://doi.org/10.5194/bg-17-1685-2020, 2020.

Jiang, L.-Q., R. A. Feely, B. R. Carter,, D. J. Greeley, D. K. G., and, and Arzayus, K. M.: Climatological distribution of aragonite saturation state in the global oceans, Global Biogeochem Cycles, 29, https://doi.org/10.1002/2015GB005198, 2015.

Lauvset, S. K., Key, R. M., Olsen, A., Heuven, S. v., A. Velo, Lin, X., C. Schirnick, Kozyr, A., T. Tanhua, Hoppema, M., Jutterström, S., R. Steinfeldt, Jeansson, E., Ishii, M., Pérez, F. F., Suzuki, T., and Watelet:, S.: A new global interior ocean mapped climatology: the 1°x1° GLODAP version 2, Earth Syst. Sci. Data, 8, 325–340, https://doi.org/10.5194/essd-8-325-2016, 2016.

Lee, K., Tong, L. T., Millero, F. J., Sabine, C. L., Dickson, A. G., Goyet, C., Park, G.-H., Wanninkhof, R., Feely, R. A., and Key, R. M.: Global relationships of total alkalinity with salinity and temperature in surface waters of the world's oceans Geophys. Res. Let., 33, L19605, https://doi.org/19610.11029/12006GL027207, 022006, 2006.

Lueker, T. J., Dickson, A. G., and Keeling, C. D.: Ocean $pCO_2$ calculated from dissolved inorganic carbon, alkalinity, and equations for K1 and K2; validation based on laboratory measurements of $CO_2$ in gas and seawater at equilibrium, Mar. Chem., 70, 105-119, 2000.

McGillis, W., and Wanninkhof, R.: Aqueous CO2 gradients for air-sea flux estimates, Marine Chemistry, 98, 100-108, 2006.

Millero, F. J., Lee, K., and Roche, M.: Distribution of alkalinity in the surface waters of the major oceans, Mar. Chem., 60, 111-130, 1998.

Minnett, P. J., Knuteson, R. O., Best, F. A., Osborne, B. J., Hanafin, J. A., and Brown, O. B.: The Marine-Atmospheric Emitted Radiance Interferometer: A high-accuracy, seagoing infrared spectroradiometer, Journal of Atmospheric and Oceanic Technology, 18, 994-1013, https://doi.org/10.1175/1520-0426, 2001.

Mollica, N. R., Guo, W., Cohen, A. L., Huang, K.-F., Foster, G. L., Donald, H. K., and Solow, A. R.: Ocean acidification affects coral growth by reducing skeletal density, Proceedings of the National Academy of Sciences, 115, 1754, https://doi.org/10.1073/pnas.1712806115, 2018.

Mucci, A.: The solubility of calcite and aragonite in seawater at various salinities, temperatures, and one atmosphere total pressure, Am. J. of Science, 283, 780-799, https://doi.org/10.2475/ajs.283.7.780, 1983.

Nojiri, Y. S. N., C. Miyazaki, F. Shimano,T. Egashira, K. Kinoshita, H. Kimoto, and A. Dickson, Ocean $pCO_2$ System Inter-comparison at Hasaki, Japan on Feb. 2009, personal communication 2009.

Orr, J. C., Epitalon, J.-M., Dickson, A. G., and Gattuso, J.-P.: Routine uncertainty propagation for the marine carbon dioxide system, Marine Chemistry, 207, 84-107, https://doi.org/10.1016/j.marchem.2018.10.006, 2018.

Perez, F. F., and Fraga, F.: A precise and rapid analytical procedure for alkalinity determination, Mar. Chem., 21, 169-182, 1987.

Pierrot, D., Lewis, E., and Wallace, D. W. R.: MS Excel program developed for CO2 system calculations, ORNL/CDIAC-105a. ed., Carbon Dioxide Information Analysis Center, Oak Ridge National Laboratory, U.S. Department of Energy, Oak Ridge, Tennessee. https://doi.org/ 10.3334/CDIAC/otg.CO2SYS_XLS_CDIAC105a, 2006.

Pierrot, D., Neil, C., Sullivan, K., Castle, R., Wanninkhof, R., Lueger, H., Johannson, T., Olsen, A., Feely, R. A., and Cosca, C. E.: Recommendations for autonomous underway $pCO_2$ measuring systems and data reduction routines, Deep -Sea Res II, 56, 512-522, 2009.

Purkis, S., Cavalcante, G., Rohtla, L., Oehlert, A., Harris, P.M., and Swart, P.: Hydrodynamic control of whitings on Great Bahama Bank, Geology, 45(10), 939-942, https://doi.org/10.1130/G39369.1, 2017.

Reynolds, R. W., Smith, T. M., Liu, C., Chelton, D. B., Casey, K. S., and Schlax, M. G.: Daily high-resolution blended analyses for sea surface temperature, *J. Climate*, 20, 5473-5496, 2007.

Riley, J. P., and Tongudai, M.: The major cation/chlorinity ratios in sea water, Chemical Geology, 2, 263-269, https://doi.org/10.1016/0009-2541(67)90026-5, 1967.

Schuster, U., McKinley, G., Bates, N., Chevalier, F., Doney, S. C., Fay, A. R., Gonzalez-Davila, M., Gruber, N., Jones, S., Landschützer, P., Lefevre, N., Manizza, M., Mathis, J. T., Metzl, N., Olsen, A., Santana-Casiano, J. M., Takahashi, T., Wanninkhof, R., and Watson, A.: Atlantic and Artic Sea-air $CO_2$ fluxes, 1990-2009, Biogeosciences Discuss., 9, 10669-10724, https://doi.org/10.5194/bgd-9-10669-2012, 2012.

Takahashi, T., Sutherland, S. C., Chipman, D. W., Goddard, J. C., Ho, C., Newberger, T., Sweeney, C., and Munro, D. W.: Climatological distributions of pH, $pCO_2$, total $CO_2$, alkalinity, and $CaCO_3$ saturation in the global surface ocean, and temporal changes at selected locations, Mar. Chem., 164, 95-125, http://dx.doi.org/10.1016/j.marchem.2014.06.004, 2014.

Takahashi, T., Sutherland, S. C., and Kozyr, A.: Global Ocean Surface Water Partial Pressure of $CO_2$ Database: Measurements Performed During 1957-2017 (LDEO Database Version 2017) (NCEI Accession 0160492). Version 4.4. NOAA National Centers for Environmental Information. LDEOv2017, 2018.

Takahashi, T., Sutherland, S. C., Wanninkhof, R., Sweeney, C., Feely, R. A., Chipman, D. W., Hales, B., Friederich, G., Chavez, F., Sabine, C., Watson, A., Bakker, D. C. E., Schuster, U., Metzl, N., Inoue, H. Y., Ishii, M., Midorikawa, T., Nojiri, Y., Koertzinger, A., Steinhoff, T., Hoppema, M., Olafsson, J., Arnarson, T. S., Tilbrook, B., Johannessen, T., Olsen, A., Bellerby, R., Wong, C. S., Delille, B., Bates, N. R., and de Baar, H. J. W.: Climatological mean and decadal change in surface

ocean $pCO_2$, and net sea-air $CO_2$ flux over the global oceans, Deep -Sea Res II, 2009, 554-577, https://doi.org/10.1016/j.dsr2.2008.12.009, 2009.

Uppström, L. R.: The boron/chloronity ratio of deep-sea water from the Pacific Ocean, Deep-Sea Research, 21, 161-162, 1974.

Wanninkhof, R., Pierrot, D., Sullivan, K.F., Barbero, L., Triñanes, J. A. A 17-year dataset of surface water fugacity of carbon dioxide ($fCO_2$), along with calculated pH, aragonite saturation state, and air-sea $CO_2$ fluxes in the Caribbean Sea, Gulf of Mexico and North-East Atlantic Ocean covering the timespan from 2003-03-01 to 2018-12-31, (NCEI Accession 0207749). NOAA National Centers for Environmental Information. Dataset. https://accession.nodc.noaa.gov/0207749. Accessed [date]. https://doi.org/10.25921/2swk-9w56, 2019a

Wanninkhof, R., Triñanes, J., Park, G.-H., Gledhill, D., and Olsen, A.: Large decadal changes in air-sea $CO_2$ fluxes in the Caribbean Sea. Journal of Geophysical Research, Oceans ,124 . https://doi.org/10.1029/2019JC015366. 2019b.

Wanninkhof, R.: Relationship between wind speed and gas exchange over the ocean revisited, Limnol and Oceanogr: Methods, 12, 351-362, https://doi.org/10.4319/lom.2014.12.351, 2014.

Wanninkhof, R., Bakker, D., Bates, N., Olsen, A., and Steinhoff, T.: Incorporation of alternative sensors in the SOCAT database and adjustments to dataset quality control flags, Carbon Dioxide Information Analysis Center, Oak Ridge National Laboratory, US Department of Energy, Oak Ridge, Tennessee, 25, https://doi.org/10.3334/CDIAC/OTG.SOCAT_ADQCF, 2013.

Webb, J. R., Maher, D. T., and Santos, I. R.: Automated, in situ measurements of dissolved $CO_2$, $CH_4$, and $\delta^{13}C$ values using cavity enhanced laser absorption spectrometry: Comparing response times of air-water equilibrators, Limnology and Oceanography: Methods, 14, 323-337, https://doi.org/10.1002/lom3.10092, 2016.

Weiss, R. F.: Carbon dioxide in water and seawater: the solubility of a non-ideal gas, Mar. Chem., 2, 203-215, 1974.

Weiss, R. F., and Price, B. A.: Nitrous oxide solubility in water and seawater, Mar. Chem., 8, 347-359, 1980.

Wilkinson, M. D., Dumontier, M., Aalbersberg, I. J., Appleton, G., Axton, M., Baak, A., Blomberg, N., Boiten, J.-W., da Silva Santos, L. B., Bourne, P. E., Bouwman, J., Brookes, A. J., Clark, T., Crosas, M., Dillo, I., Dumon, O., Edmunds, S., Evelo, C. T., Finkers, R., Gonzalez-Beltran, A., Gray, A. J. G., Groth, P., Goble, C., Grethe, J. S., Heringa, J., 't Hoen, P. A. C., Hooft, R., Kuhn, T., Kok, R., Kok, J., Lusher, S. J., Martone, M. E., Mons, A., Packer, A. L., Persson, B., Rocca-Serra, P., Roos, M.,

van Schaik, R., Sansone, S.-A., Schultes, E., Sengstag, T., Slater, T., Strawn, G., Swertz, M. A., Thompson, M., van der Lei, J., van Mulligen, E., Velterop, J., Waagmeester, A., Wittenburg, P., Wolstencroft, K., Zhao, J., and Mons, B.: The FAIR Guiding Principles for scientific data management and stewardship, Scientific Data, 3, 160018, https://doi.org/10.1038/sdata.2016.18, 2016.

Woolf, D. K., Land, P. E., Shutler, J. D., Goddijn-Murphy, L. M., and Donlon, C. J.: On the calculation of air-sea fluxes of $CO_2$ in the presence of temperature and salinity gradients, Journal of Geophysical Research: Oceans, 121, 1229-1248, https://doi.org/10.1002/2015JC011427, 2016.

695

**Figure captions**

Figure 1. Map with the cruise tracks of the *EoS*, *Eqnx*, and *ALoS* from 2002 though 2018. The grayscales show bathymetry with white being less than 200-m. The green rectangle depicts the region where the data and products are compared
700 in Figure 4.

Figure 2. Histogram of number of cruises per year used in this work.

Figure 3. The difference between $fCO_{2wMLR}$ for subsequent months plotted versus time. The solid squares are the differences between December and January where different MLRs are used.

Figure 4. Zonal section of gridded and mapped products between 23˚ N and 24˚ N for January 2004 (Black), January 2011
705 (Blue), and January 2017 (Red). a. $fCO_{2w}$; b. SST; c. SSS. The lines with small solid circles are the mapped product, the larger solid circles are the gridded data with standard deviation of data in the box shown as error bars.

Figure 5. Relationships of surface water TA with salinity. The relationship of Cai et al. (2010), with standard error shown as error bars, is used to calculate pH and $\Omega_{Ar}$ from $fCO_{2w}$.

Figure 6. $pH_T$ calculated from gridded $fCO_{2w}$ and TA estimated from SSS, $pH_T(fCO_2,TA)$, as done in this work, minus $pH_T$
710 calculated from observed $fCO_{2w}$ and TA from SSS, $pH_T(MLR)$ plotted against temperature for the 2017 data.

Appendix A

# A 17-year dataset of surface water fugacity of $CO_2$, along with calculated pH, Aragonite saturation state, and air-sea $CO_2$ fluxes in the Caribbean Sea

Rik Wanninkhof, Denis Pierrot, Kevin Sullivan, Leticia Barbero, and Joaquin Triñanes

Multi-linear regressions (MLRs) for $fCO_{2w}$ were applied to the data on a (1˚ by 1˚ by mo) grid using sequentially fewer independent parameters and the increase in residual was determined. This analysis was performed as two of the independent parameters used, sea surface salinity, SSS and mixed layer depth, MLD, are modeled and their accuracy is not readily known. The functional form for the multi-linear regression, MLR fit is:

$$fCO_{2w,MLR} = a\ Lon + b\ Lat + c\ SST + [d\ MLD] + [e\ SSS] + f \quad (A1)$$

Lon is longitude; Lat is latitude, and SST is sea surface temperature. The MLR with the full number of independent parameters are used in the data products described the main text and the resulting data products are in Wanninkhof et al. (2019a). The terms in brackets indicate the parameters omitted in the estimates here. The coefficients for the MLRs and their standard errors for each year without MLD, and the MLRs without MLD and SSS, are provided in Tables A1 and A2. SST and location are the strongest predictors of $fCO_{2w}$ levels in the region. The increase in the average root mean square of the residual/error (RMSE) excluding MLD and SSS in the annual MLRs is shown in Tables A1 and A2. The average RMSE of the calculated $fCO_{2w,MLR}$ increases by 8 ± 5.5 % by excluding MLD, and increases by 11 ± 5.4 % when MLD and SSS are omitted with the annual differences provided in the last column of Tables A1 and A2.

For the entire record, from 2002-2018, single regressions of $fCO_{2w}$ with position, SST, SSS, and MLD showed larger standard errors and coefficients of determination ($r^2$) as they do not capture the increase in $fCO_{2w}$ over time due to $fCO_{2w}$ increases in response to increasing atmospheric $CO_2$ levels. Regressing against $\Delta fCO_2$ which, in principle should not have a trend over time if surface water $CO_2$ levels keep up with atmospheric $CO_2$ increases, did not improve the correlation with the independent parameters. This was attributed to the relatively small magnitude of $\Delta fCO_2$ and the observed multi-year changes in trends of $fCO_{2w}$ (Wanninkhof et al., 2019b). However, using the year as a variable in the regression provides a reasonable means of extrapolating over the entire time/space domain with a single regression from 3/2002 through 2/2018:

$$fCO_{2w,MLR}\ (\pm 7.8) = 23.3\ (\pm 2.0) + 1.45\ (\pm 0.02)\ (YR-2002) + 10.23\ (\pm 0.06)\ SST + 1.19\ (\pm 0.03)\ Lat - 0.50\ (\pm 0.01)\ Lon, \quad r^2 = 0.84 \quad (A2)$$

where YR is the integer calendar year. Thus (YR-2002) is the year since the start of the record. The coefficient for the (YR-2002) term of 1.45 reflects the annual increase in surface water $fCO_{2w}$ due to atmospheric $fCO_{2a}$ increase, which averages 2.1 µatm $yr^{-1}$ over the 2002-2018 time period.

The standard error in the $fCO_{2w,MLR}$ of 7.8 µatm in Eq. A2 is generally greater than the standard error in the annual algorithms used to fill the gaps for the annual estimates (Eq. A1) that range from 4.7 to 9.9 µatm depending on the year with an average of 6.4 µatm (Table 1 in main text).

The importance of the different independent variables for the $fCO_{2w,MLR}$ can, in part, be discerned from the standard error in the coefficients but since variables are cross-correlated, other means are investigated such as creating a MLR with either a subset or substitution of variables. Physical parameters were correlated with location (Lat, Lon) in the region. In particular, salinity showed broad correspondence with position. Therefore, substituting SSS for Lat and Lon provided similar magnitude and standard error in the coefficients of the independent variable, but a 10 % greater RMS in the estimated $fCO_{2w}$:

$$fCO_{2w,MLR}\ (\pm 8.8) = -238\ (\pm 9.8) + 1.36\ (\pm 0.02)\ (YR-2002) + 10.11\ (\pm 0.06)\ SST + 9.07\ (\pm 0.25)\ SSS,\ r^2 = 0.79 \quad (A3)$$

Finally, a simple two parameter linear fit with YR and SST had reasonable predictive capability:

$$fCO_{2w,MLR}\ (\pm 9.4) = 107.2\ (\pm 1.7) + 1.38\ (\pm 0.02)\ (YR-2002) + 9.50\ (\pm 0.06)\ SST \qquad r^2 = 0.77 \qquad (A4)$$

Eq. A4 which used only SST and time showed an increase in the standard error of the derived independent variable $fCO_{2w}$ compared to the other permutations of the MLR. This simple relationship did show some biases with location (not shown), and for gap filling to create uniform monthly fields of $fCO_{2w}$ the full annual regressions (Table 1) using all independent parameters, SST, SSS, MLD and location was the best option.

**Table A1**. Coefficients for the MLR, $fCO_{2w,MLR} = a\ Lon + b\ Lat + c\ SST + e\ SSS + f$

**Table A2**. Coefficients for the MLR, $fCO_{2w,MLR} = a\ Lon + b\ Lat + c\ SST + f$

**References Appendix A**

Wanninkhof, R., Pierrot, D., Sullivan, K.F., Barbero, L., Triñanes, J. A. A 17-year dataset of surface water fugacity of carbon dioxide ($fCO_2$), along with calculated pH, aragonite saturation state, and air-sea $CO_2$ fluxes in the Caribbean Sea, Gulf of Mexico and North-East Atlantic Ocean covering the timespan from 2003-03-01 to 2018-12-31, (NCEI Accession 0207749).

NOAA National Centers for Environmental Information. Dataset. https://accession.nodc.noaa.gov/0207749. Accessed [date]. https://doi.org/10.25921/2swk-9w56, 2019a

Wanninkhof, R., Triñanes, J., Park, G.-H., Gledhill, D., and Olsen, A.: Large decadal changes in air-sea $CO_2$ fluxes in the Caribbean Sea. Journal of Geophysical Research, Oceans ,124 . https://doi.org/10.1029/2019JC015366. 2019b.

785

**Table 1**. Coefficients for the MLR for each year*

| | a (LON) | b (LAT) | c (SST) | d (MLD) | e (SSS) | f (Icept) | Standard error $fCO_{2w,MLR}$ | $r^2$ | #points |
|---|---|---|---|---|---|---|---|---|---|
| 2002 | -0.32 | 0.45 | 10.29 | -0.04 | 0.77 | 24.4 | 4.72 | 0.90 | 537 |
| | *0.04* | *0.11* | *0.18* | *0.02* | *0.72* | *25.8* | | | |
| 2003 | -0.56 | 0.32 | 9.24 | -0.09 | 1.11 | 32.6 | 5.21 | 0.86 | 731 |
| | *0.03* | *0.09* | *0.17* | *0.02* | *0.66* | *24.6* | | | |
| 2004 | -0.42 | 0.82 | 10.34 | -0.20 | 2.78 | -55.4 | 5.21 | 0.92 | 740 |
| | *0.03* | *0.09* | *0.17* | *0.01* | *0.63* | *23.6* | | | |
| 2005 | -0.43 | 0.49 | 8.71 | -0.07 | 7.30 | -172.0 | 6.58 | 0.85 | 664 |
| | *0.04* | *0.12* | *0.18* | *0.02* | *0.85* | *32.1* | | | |
| 2006 | -0.31 | 1.13 | 9.60 | -0.19 | 2.56 | -26.6 | 4.99 | 0.89 | 670 |
| | *0.03* | *0.08* | *0.16* | *0.02* | *0.70* | *26.1* | | | |
| 2007 | -0.62 | 1.12 | 10.56 | -0.36 | 2.75 | -77.8 | 7.04 | 0.79 | 483 |
| | *0.05* | *0.15* | *0.32* | *0.03* | *1.33* | *49.0* | | | |
| 2008 | -0.12 | 1.12 | 10.58 | -0.30 | 3.16 | -55.8 | 5.66 | 0.95 | 107 |
| | *0.43* | *0.31* | *0.45* | *0.05* | *1.39* | *59.8* | | | |
| 2009 | -0.66 | 0.30 | 7.18 | -0.47 | 0.11 | 131.9 | 6.91 | 0.84 | 125 |
| | *0.22* | *0.24* | *0.53* | *0.07* | *1.49* | *58.8* | | | |
| 2010 | -0.53 | 2.02 | 8.48 | -0.23 | 2.12 | -10.5 | 9.31 | 0.85 | 323 |
| | *0.17* | *0.26* | *0.41* | *0.05* | *1.48* | *51.7* | | | |
| 2011 | -0.32 | 0.98 | 6.65 | -0.28 | 3.06 | 46.8 | 7.19 | 0.76 | 305 |
| | *0.13* | *0.19* | *0.34* | *0.04* | *1.51* | *59.7* | | | |
| 2012 | -0.13 | 1.66 | 10.81 | -0.33 | 5.56 | -154.1 | 7.29 | 0.91 | 358 |
| | *0.10* | *0.16* | *0.28* | *0.04* | *1.36* | *50.9* | | | |
| 2013 | -0.43 | 1.30 | 11.45 | -0.47 | 4.45 | -137.5 | 8.16 | 0.83 | 219 |
| | *0.18* | *0.23* | *0.48* | *0.05* | *1.63* | *55.5* | | | |
| 2014 | -0.60 | 0.62 | 9.48 | -0.18 | 3.26 | -45.2 | 7.02 | 0.78 | 362 |
| | *0.08* | *0.15* | *0.29* | *0.03* | *1.06* | *37.7* | | | |
| 2015 | -0.84 | 0.14 | 7.76 | -0.18 | 1.20 | 70.0 | 6.01 | 0.82 | 455 |
| | *0.04* | *0.11* | *0.27* | *0.02* | *0.90* | *34.5* | | | |

| | | | | | | | | | |
|---|---|---|---|---|---|---|---|---|---|
| 2016 | -0.79 | 0.37 | 8.72 | -0.14 | 4.17 | -62.7 | 6.66 | 0.82 | 1001 |
| | *0.03* | *0.08* | *0.20* | *0.01* | *0.45* | *17.1* | | | |
| 2017 | -0.42 | 0.56 | 9.49 | -0.22 | 5.65 | -112.6 | 6.17 | 0.87 | 974 |
| | *0.03* | *0.08* | *0.15* | *0.02* | *0.58* | *17.1* | | | |
| 2018 | -0.34 | -0.09 | 10.85 | -0.13 | 6.24 | -151.2 | 5.08 | 0.90 | 1162 |
| | *0.02* | *0.07* | *0.13* | *0.01* | *0.39* | *14.7* | | | |

* These annual regressions were used to create the mapped $fCO_{2wMLR}$ fields using the 1˚ by 1˚ by month gridded data product.

$fCO_{2wMLR}$ = a Longitude + b Latitude + c OISST + d $MLD_{Hycom}$ + e $SSS_{Hycom}$ + f

The second row (in italics) for each annual entry is the error of the coefficient.

**Table 2.** Estimated uncertainties in measured, gridded, and mapped variables

| Parameter | Method* | Combined Standard Uncertainty | Systematic Uncertainty** |
|---|---|---|---|
| $fCO_{2w}$ | Measured | 2 µatm | |
| SSS | Measured | 0.1 per mil | |
| SST | Measured | 0.02 ˚C | |
| $fCO_{2w}$ | Gridded | 3.4 µatm | |
| SSS | Gridded | 0.10 per mil | |
| SST | Gridded | 0.22 ˚C | |
| TA | Gridded/Calculated | 8 µmol $kg^{-1}$ | |
| $pH_T$ | Gridded/Calculated | 0.0075 | |
| $\Omega_{Ar}$ | Gridded/Calculated | 0.2 | |
| $fCO_{2wMLR}$ | Mapped/MLR | 6.4 µatm | Gridded $fCO_{2w}$-$fCO_{2wMLR}$= 1.5 µatm |
| $SSS_{Hycom}$ | Model | 0.2 | Gridded SSS-$SSS_{Hycom}$= -0.1 |
| OISST | Interpolated/remote sensing | 0.2 ˚C | Gridded SST- OISST= 0.24˚C |
| TA | Mapped/Calculated | 7.9 µmol $kg^{-1}$ | $TA_{SSS}$-$TA_{SSSHycom}$=-5.25 µmol $kg^{-1}$ |
| $pH_T$ | Mapped/Calculated | .009 | pH(TA,$fCO_{2w}$) – $pH_T$(MLR)= 0.002 |
| $\Omega_{Ar}$ | Mapped/Calculated | 0.21 | 0.004 |
| Flux $CO_2$ | Mapped/Calculated | 0.18 mol $m^{-2}$ $yr^{-1}$ | $Flux_{SST}$- Flux OISST =0.24 mol $m^{-2}$ $yr^{-1}$ |

*Method refers to either the individual data point (measured); the values averaged on a 1˚ by1˚ by mo (gridded); or the interpolated products (mapped).

**The systematic uncertainty is based on the difference between the different methods and products as indicated.

Note, the combined standard uncertainties and systematic uncertainties are based on average conditions

800 **Table 3.** Column headers for the monthly 1-degree gridded observational product (1˚ by 1˚ by mo)

| Parameter | Unit | Description |
|---|---|---|
| Year | | |
| Month | | 1 (January) through 12 (December) |
| Latitude (Lat) | Degrees | North is positive. Location is the center point of the grid cell. That is, 15.5˚ N is the grid box spanning 15˚ N to 16˚ N |
| Longitude (Lon) | Degrees | East is positive. All values in the Caribbean are negative. Location is center point of the grid cell. That is, -87.5 is the grid box spanning 87˚ W to 88˚ W |
| Area | $Km^2$ | Area of grid box excluding land where appropriate |
| #_Obs | | Number of $fCO_{2w}$ observations in the particular grid box for the particular month |
| SST_OBS | ˚C | Sea surface temperature measured at the intake (average of the grid box) |
| SST_STDEV | ˚C | Standard deviation of SST |
| SSS_OBS | permil | Sea surface salinity measured by thermosalinograph (average of the grid box) |
| SSS_STDEV | permil | Standard deviation of SSS |
| $fCO_{2w}$_OBS | µatm | Fugacity of $CO_2$ in seawater (average of the grid box) |
| $fCO_{2w}$_STDEV | µatm | Standard deviation of $fCO_{2w}$ observations in the grid box |
| TA | µmol $kg^{-1}$ | Total alkalinity calculated from a relationship salinity TA = 57.3SSS_OBS+ 296.4 (Cai et al., 2010) using the measured SSS |
| $pH_T$ | | pH on the total scale at SST calculated from $fCO_{2w}$_OBS and TA using the CO2SYS program of Pierrot et al. (2006) with pH Scale: Total scale (mol/kg-SW) at OISST; $CO_2$ Constants: K1, K2 from Lueker et al. (2000); $KSO_4^-$ for Dickson (1990); KF from Perez and Fraga (1987) and Total Boron from Uppström (1974) |
| $\Omega_{Ar}$ | | Aragonite saturation state calculated using CO2SYS with $fCO_{2w}$_OBS and TA as input parameters and the same dissociation constants as used for $pH_T$ |
| OISST | ˚C | Optimal interpolated sea surface temperature (Reynolds et al., 2007) for the particular grid box |
| $SSS_{HYCOM}$ | permil | Sea surface salinity from the HYCOM model |
| $fCO_{2wMLR}$ | µatm | Fugacity of $CO_2$ in seawater determined from annual MLRs (see Table 1) with Lat, Lon, SST, OISST, $SSS_{HYCOM}$, and $MLD_{HYCOM}$. |

**Table 4.** Column headers for the monthly 1-degree mapped product (1˚ by 1˚ by mo) for the whole region

| Parameter | Unit | Description |
|---|---|---|
| Year | | |
| Month | | 1 (January) through 12 (December) |
| Latitude (Lat) | Degrees | North is positive. Location is center point of the grid cell. For example, 15.5˚ N is the grid box spanning 15˚ N to 16˚ N |
| Longitude (Lon) | Degrees | East is positive. All values in Caribbean are negative. Location is center point of the grid cell. For example, -87.5 is the grid box spanning 87˚ W to 88˚ W |
| Area | $Km^2$ | Area of grid box excluding land where appropriate |
| OISST | ˚C | Optimal interpolated sea surface temperature (Reynolds et al., 2007) |
| $SSS_{HYCOM}$ | permil | Sea surface salinity Sea surface salinity from HYCOM |
| $MLD_{HYCOM}$ | m | Mixed layer depth from the HYCOM model |
| $fCO_{2wMLR}$ | µatm | Fugacity of $CO_2$ in seawater determined from annual MLRs with Lat, Lon, SST, SSS, and MLD (see Table 1) |
| $fCO_{2a}$ | µatm | Fugacity of $CO_2$ in air using the average value between atmospheric sampling station KEY and RBP |
| $\Delta fCO_2$ | µatm | Air water fugacity difference, $fCO_{2w}$ - $fCO_{2a}$ |
| TA | µmol $kg^{-1}$ | Total alkalinity calculated from a relationship salinity TA = $57.3SSS_{HYCOM}$+ 296.4 (Cai et al., 2010) |
| $pH_T$ | | pH calculated from $fCO_{2w}$ and TA with the CO2SYS program of Pierrot et al. (2006) with pH Scale: Total scale (mol/kg-SW) at OISST; $CO_2$ Constants: K1, K2 from Lueker et al. (2000); $KSO_4^-$ for Dickson (1990); KF from Perez and Fraga (1987) and Total Boron from Uppström (1974) |
| $\Omega_{Ar}$ | | Aragonite saturation state calculated using CO2SYS with $fCO_{2wMLR}$, TA, OISST, and $SSS_{HYCOM}$ as input parameters with same dissociation constants as used for $pH_T$ |
| $<u^2>$ | $m^2$ $s^{-2}$ | Second moment of the wind based on ¼˚ 6-h CCMP-2 product (Atlas et al., 2011) |
| $CO_2$_Flux | mol $m^{-2}$ $yr^{-1}$ | Monthly air-sea $CO_2$ flux calculated according to Eqs. 5 and 6, with $fCO_{2wMLR}$ @ OISST |

805

**Table 5.** Column headers for the monthly averaged mapped product

| Parameter | Unit | Description |
|---|---|---|
| Year | | |
| Month | | 1 (January) through 12 (December) |
| Area | $km^2$ | Total area of Caribbean region excluding land (15˚ N to 28˚ N and 62˚ W to 88˚ W) |
| OISST | ˚C | Optimal interpolated sea surface temperature (Reynolds et al., 2007) |
| $SSS_{HYCOM}$ | permil | Sea surface salinity Sea surface salinity from HYCOM |
| $MLD_{HYCOM}$ | m | Mixed layer depth from the HYCOM model |
| $fCO_{2wMLR}$ | µatm | Fugacity of $CO_2$ in seawater determined from annual MLRs with Lat, Lon, SST, SSS, and MLD (see Table 1) |
| $fCO_{2a}$ | µatm | Fugacity of $CO_2$ in air using the average value between atmospheric sampling station KEY and RBP |
| $\Delta fCO_2$ | µatm | Air-water fugacity difference, $fCO_{2w}$ - $fCO_{2a}$ |
| TA | µmol $kg^{-1}$ | Total alkalinity calculated from a relationship salinity TA = $57.3SSS_{HYCOM}$+ 296.4 (Cai et al., 2010) |
| $pH_T$ | | pH calculated from $fCO_{2w}$ and TA with the CO2SYS program of Pierrot et al. (2006) with pH Scale: Total scale at OISST; $CO_2$ Constants: K1, K2 from Lueker et al. (2000); $KSO_4^-$ for Dickson (1990); KF from Perez and Fraga (1987) and Total Boron from Uppström (1974) |
| $\Omega_{Ar}$ | | Aragonite saturation state calculated using CO2SYS with $fCO_{2wMLR}$, TA, OISST, and $SSS_{HYCOM}$ as input parameters with same dissociation constants as used for $pH_T$ |
| $<u^2>$ | $m^2$ $s^{-2}$ | Second moment of the wind based on ¼˚ 6-h CCMP-2 product (Atlas et al., 2011) |
| $CO_2$_Flux | mol $m^{-2}$ $mo^{-1}$ | Monthly air-sea $CO_2$ flux calculated according to Eqs. 5 and 6 |
| $CO_2$_$Flux_{Total}$ | Tg C $mo^{-1}$ | Total monthly air-sea $CO_2$ flux calculated according to Eqs. 5 and 6 in Teragram carbon |

**Table 6.** Column headers for the annual averaged mapped product

| | | |
|---|---|---|
| Year | | |
| Area | $km^2$ | Total area of Caribbean region, excluding land, from 15˚ N to 28˚ N and 62˚ W to 88˚ W |
| OISST | ˚C | Optimal interpolated sea surface temperature (Reynolds et al., 2007) |
| $SSS_{HYCOM}$ | permil | Sea surface salinity Sea surface salinity from HYCOM |
| $MLD_{HYCOM}$ | m | Mixed layer depth from the HYCOM model |
| Area | $Km^2$ | Area of grid box excluding the surface area of land where appropriate |
| $fCO_{2wMLR}$ | µatm | Fugacity of $CO_2$ in seawater determined from annual MLRs with Lat, Lon, SST, SSS, and MLD (see Table 1) |
| $fCO_{2a}$ | µatm | Fugacity of $CO_2$ in air using the average value between atmospheric sampling station KEY and RBP |
| $\Delta fCO_2$ | µatm | Air water fugacity difference, $fCO_{2w}$ - $fCO_{2a}$ |
| TA | µmol $kg^{-1}$ | Total alkalinity calculated from a relationship salinity TA = $57.3SSS_{HYCOM}$+ 296.4 (Cai et al., 2010) |
| $pH_T$ | | pH calculated from $fCO_{2w}$ and TA with the CO2SYS program of Pierrot et al. (2006) with pH Scale: Total scale at OISST; $CO_2$ Constants: K1, K2 from Lueker et al. (2000); $KSO_4^-$ for Dickson (1990); KF from Perez and Fraga (1987) and Total Boron from Uppström (1974) |
| $\Omega_{Ar}$ | | Aragonite saturation state calculated using CO2SYS with $fCO_{2wMLR}$, TA, OISST, and $SSS_{HYCOM}$ as input parameters with same dissociation constants as used for $pH_T$ |
| $<u^2>$ | $m^2$ $s^{-2}$ | Second moment of the wind based on ¼˚ 6-h CCMP-2 product (Atlas et al., 2011) |
| $CO_2$_Flux | mol $m^{-2}$ $yr^{-1}$ | Annual air-sea $CO_2$ flux calculated according to Eqs. 5 and 6 |
| $CO_2$_$Flux_{Total}$ | Tg C $y^{-1}$ | Total annual air-sea $CO_2$ flux calculated according to Eqs. 5 and 6 in Teragram carbon |

**Table A1**. Coefficients for the MLR, $fCO_{2w,MLR}$ = a Lon + b Lat + c SST + e SSS + f

| | a (Lon) | b (Lat) | c (SST) | f (Icept) | RMSE $fCO_{2w,MLR}$ | $r^2$ | #points | % increase RMSE** |
|---|---|---|---|---|---|---|---|---|
| 2002 | -0.30 | 0.48 | 10.42 | 16.6 | 4.74 | 0.90 | 537 | 0.4 |
| * | *0.04* | *0.11* | *0.17* | *25.7* | | | | |
| 2003 | -0.53 | 0.35 | 9.60 | 26.7 | 5.32 | 0.86 | 731 | 2.1 |
| | *0.03* | *0.09* | *0.16* | *25.1* | | | | |
| 2004 | -0.35 | 0.89 | 11.52 | -118.3 | 5.79 | 0.90 | 740 | 11.1 |
| | *0.03* | *0.10* | *0.16* | *25.7* | | | | |
| 2005 | -0.41 | 0.53 | 9.08 | -198.3 | 6.65 | 0.85 | 664 | 1.1 |
| | *0.04* | *0.12* | *0.15* | *31.8* | | | | |
| 2006 | -0.20 | 1.26 | 10.23 | -98.5 | 5.48 | 0.87 | 670 | 9.8 |
| | *0.03* | *0.09* | *0.16* | *27.9* | | | | |
| 2007 | -0.50 | 1.33 | 12.05 | -246.0 | 7.96 | 0.74 | 483 | 13.1 |
| | *0.05* | *0.17* | *0.33* | *53.0* | | | | |
| 2008 | 0.26 | 1.77 | 12.50 | -138.3 | 6.43 | 0.94 | 107 | 13.6 |
| | *0.49* | *0.33* | *0.32* | *65.9* | | | | |
| 2009 | -0.38 | 0.24 | 9.26 | -7.8 | 7.95 | 0.79 | 125 | 15.1 |
| | *0.25* | *0.28* | *0.48* | *62.8* | | | | |
| 2010 | -0.45 | 2.43 | 10.11 | -61.4 | 9.66 | 0.84 | 323 | 3.8 |
| | *0.18* | *0.26* | *0.25* | *52.6* | | | | |
| 2011 | -0.49 | 1.03 | 8.11 | -157.1 | 7.83 | 0.71 | 305 | 8.9 |
| | *0.14* | *0.20* | *0.31* | *58.0* | | | | |
| 2012 | -0.19 | 1.95 | 12.27 | -253.6 | 8.01 | 0.89 | 358 | 9.9 |
| | *0.11* | *0.17* | *0.24* | *54.5* | | | | |
| 2013 | -0.13 | 1.89 | 13.04 | -256.5 | 9.66 | 0.76 | 219 | 18.4 |
| | *0.21* | *0.27* | *0.53* | *63.9* | | | | |
| 2014 | -0.31 | 0.96 | 9.89 | -20.1 | 7.40 | 0.76 | 362 | 5.4 |
| | *0.07* | *0.15* | *0.30* | *39.5* | | | | |
| 2015 | -0.86 | 0.09 | 7.96 | 23.8 | 6.65 | 0.78 | 455 | 10.6 |
| | *0.04* | *0.12* | *0.30* | *37.8* | | | | |

| | | | | | | | | |
|---|---|---|---|---|---|---|---|---|
| 2016 | -0.75 | 0.32 | 9.57 | -121.2 | 6.95 | 0.80 | 1001 | 4.4 |
| | *0.03* | *0.09* | *0.18* | *16.6* | | | | |
| 2017 | -0.42 | 0.56 | 9.49 | -112 | 6.16 | 0.87 | 969 | 0 |
| | *0.03* | *0.09* | *0.15* | *21.3* | | | | |
| 2018 | -0.34 | 0.009 | 11.57 | -173.2 | 5.35 | 0.89 | 1164 | 5.3 |
| | *0.02* | *0.07* | *0.12* | *15.43* | | | | |

*The second row (in italics) for each annual entry is the error of the coefficient.

** The increase in root mean square error (RMSE) of $fCO_{2w,MLR}$ compared to Table 1 that includes MLD as an input

820

**Table A2***. Coefficients for the MLR, $fCO_{2w,MLR}$ = a Lon + b Lat + c SST + f

| | a (Lon) | b (Lat) | c (SST) | f (Icept) | RSME $fCO_{2w,MLR}$ | $r^2$ | #points | % increase RMSE** |
|---|---|---|---|---|---|---|---|---|
| 2002 | -0.28 | 0.53 | 10.45 | 47.1 | 4.74 | 0.90 | 537 | 0.4 |
| *** | *0.04* | *0.10* | *0.17* | *5.3* | | | | |
| 2003 | -0.54 | 0.40 | 9.56 | 60.9 | 5.33 | 0.86 | 731 | 2.3 |
| | *0.03* | *0.09* | *0.16* | *5.2* | | | | |
| 2004 | -0.37 | 1.14 | 11.30 | 9.4 | 5.89 | 0.90 | 740 | 13.1 |
| | *0.03* | *0.09* | *0.15* | *5.0* | | | | |
| 2005 | -0.35 | 1.08 | 8.68 | 84.0 | 7.05 | 0.83 | 664 | 7.1 |
| | *0.04* | *0.11* | *0.16* | *5.9* | | | | |
| 2006 | -0.18 | 1.56 | 10.06 | 47.8 | 5.59 | 0.86 | 670 | 12.0 |
| | *0.03* | *0.07* | *0.16* | *6.4* | | | | |
| 2007 | -0.52 | 1.77 | 11.87 | -31.8 | 8.10 | 0.73 | 483 | 15.1 |
| | *0.05* | *0.13* | *0.34* | *12.8* | | | | |
| 2008 | 0.46 | 2.17 | 12.42 | 11.9 | 6.50 | 0.93 | 107 | 14.8 |
| | *0.49* | *0.30* | *0.33* | *28.4* | | | | |
| 2009 | -0.42 | 0.44 | 9.04 | 82.0 | 7.99 | 0.78 | 125 | 15.6 |
| | *0.25* | *0.24* | *0.46* | *20.3* | | | | |
| 2010 | -0.45 | 2.67 | 10.11 | 3.8 | 9.67 | 0.84 | 323 | 3.9 |
| | *0.18* | *0.18* | *0.25* | *12.4* | | | | |
| 2011 | -0.37 | 1.65 | 7.76 | 101.1 | 8.09 | 0.69 | 305 | 12.5 |
| | *0.15* | *0.16* | *0.31* | *14.9* | | | | |
| 2012 | -0.18 | 2.42 | 11.95 | -13.8 | 8.22 | 0.88 | 358 | 12.8 |
| | *0.12* | *0.14* | *0.23* | *11.0* | | | | |
| 2013 | -0.34 | 2.39 | 13.27 | -60.7 | 9.88 | 0.75 | 219 | 21.1 |
| | *0.20* | *0.22* | *0.53* | *23.5* | | | | |
| 2014 | -0.32 | 1.17 | 9.90 | 62.9 | 7.44 | 0.75 | 362 | 6.0 |
| | *0.07* | *0.12* | *0.30* | *11.6* | | | | |
| 2015 | -0.86 | 0.22 | 7.83 | 100.7 | 6.68 | 0.77 | 455 | 11.1 |

| | | | | | | | | |
|---|---|---|---|---|---|---|---|---|
| | *0.04* | *0.11* | *0.29* | *9.7* | | | | |
| 2016 | -0.70 | 0.67 | 9.84 | 52.3 | 7.37 | 0.77 | 1001 | 10.7 |
| | *0.04* | *0.08* | *0.19* | *6.3* | | | | |
| 2017 | -0.40 | 1.07 | 10.33 | 52.8 | 7.02 | 0.83 | 967 | 13.8 |
| | *0.03* | *0.08* | *0.16* | *5.32* | | | | |
| 2018 | *-0.37* | *0.48* | *11.22* | *44.94* | 5.82 | 0.87 | 1165 | 14.6 |
| | *0.026* | *0.07* | *0.13* | *4.23* | | | | |

* This table is the same as Table A1 except that MLD in addition to SSS are omitted as independent variables.

** The increase in root mean square error (RMSE) of $fCO_{2w,MLR}$ compared to Table 1 that included MLD and SSS as an independent variable.

*** The second row (in italics) for each annual entry is the error of the coefficient.

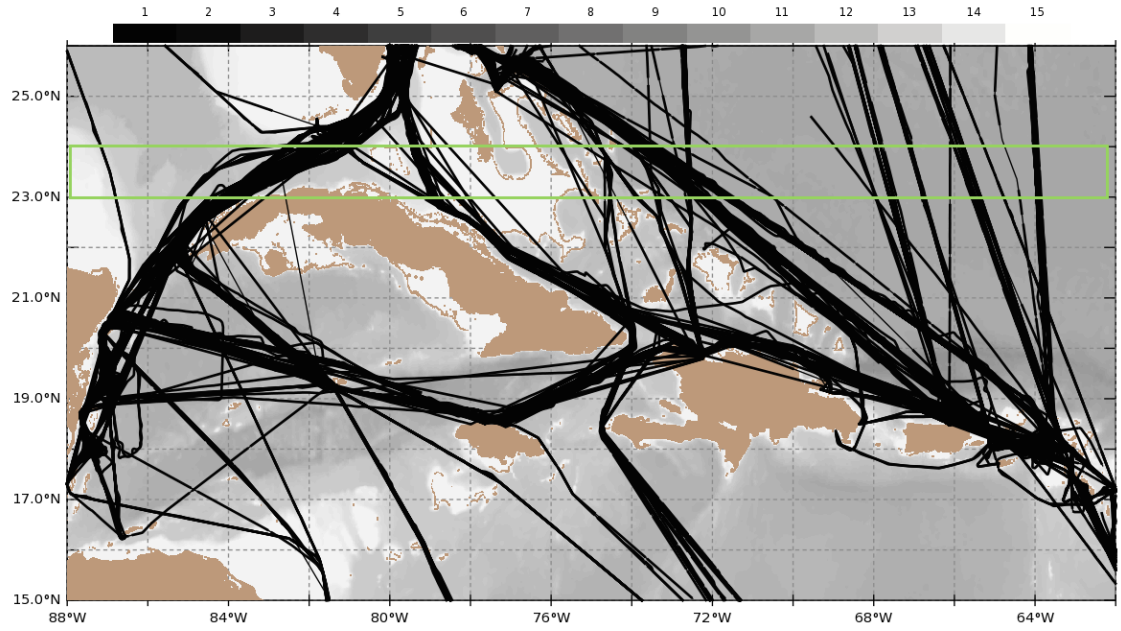
1
2
3
4
5
6
7
8
9
10
11
12
13
14
15
25.0°N
23.0°N
21.0°N
19.0°N
17.0°N
15.0°N
88°W
84°W
80°W
76°W
72°W
68°W
64°W

835

Fig 1.

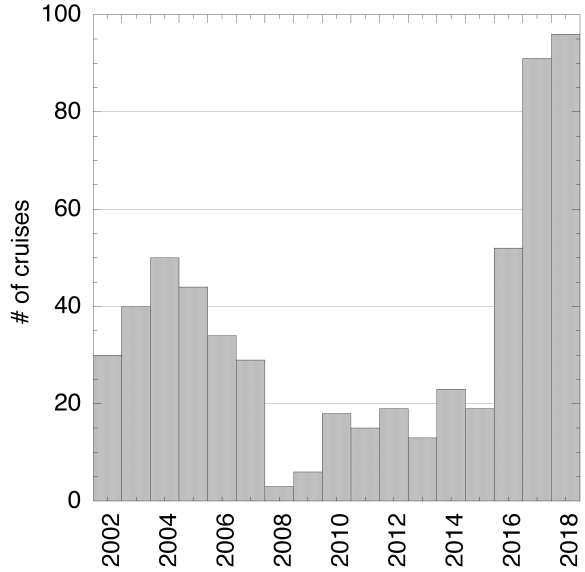
100
80
60
40
20
0
# of cruises
2002
2004
2006
2008
2010
2012
2014
2016
2018

Fig 2.

850

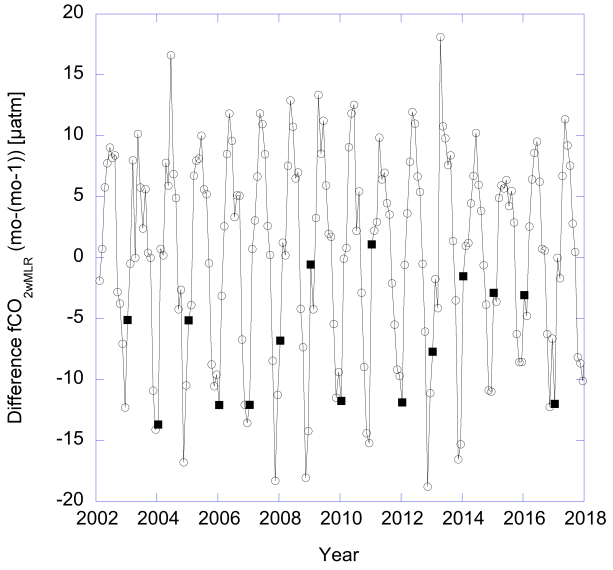
Difference fCO2wMLR (mo-(mo-1)) [µatm]
20
15
10
5
0
-5
-10
-15
-20
2002
2004
2006
2008
2010
2012
2014
2016
2018
Year

Fig. 3

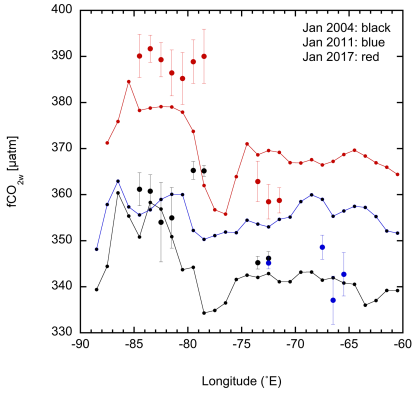


Fig. 4a

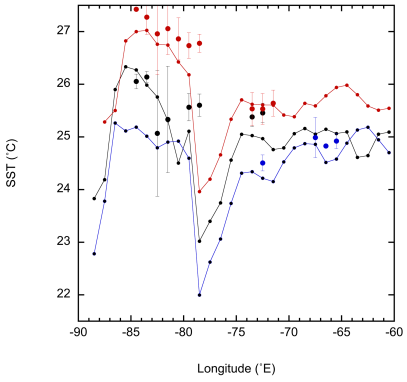


855

Fig. 4b

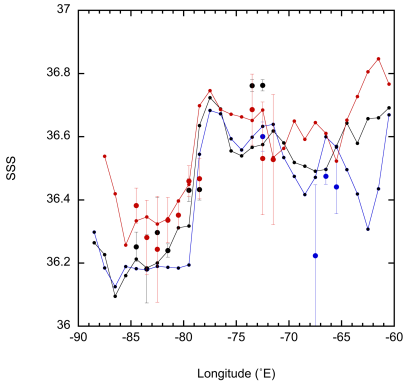


Fig. 4c

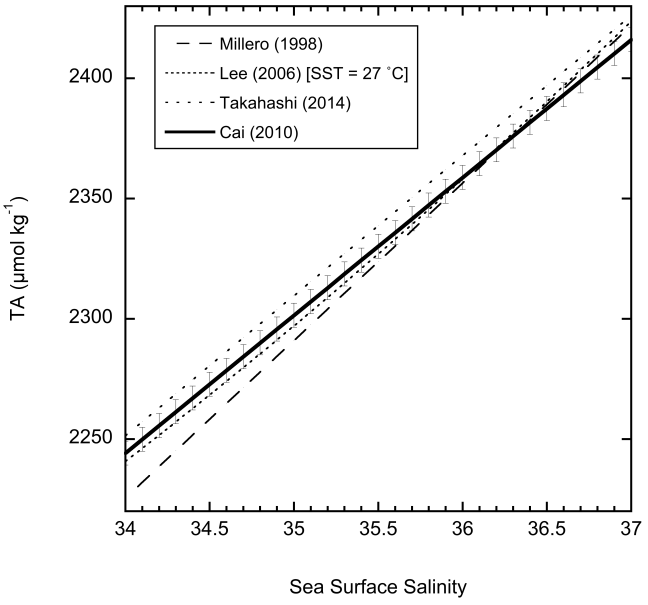
Millero (1998)
Lee (2006) [SST = 27 °C]
Takahashi (2014)
Cai (2010)
TA (μmol kg-1)
2400
2350
2300
2250
34
34.5
35
35.5
36
36.5
37
Sea Surface Salinity

860

Fig. 5

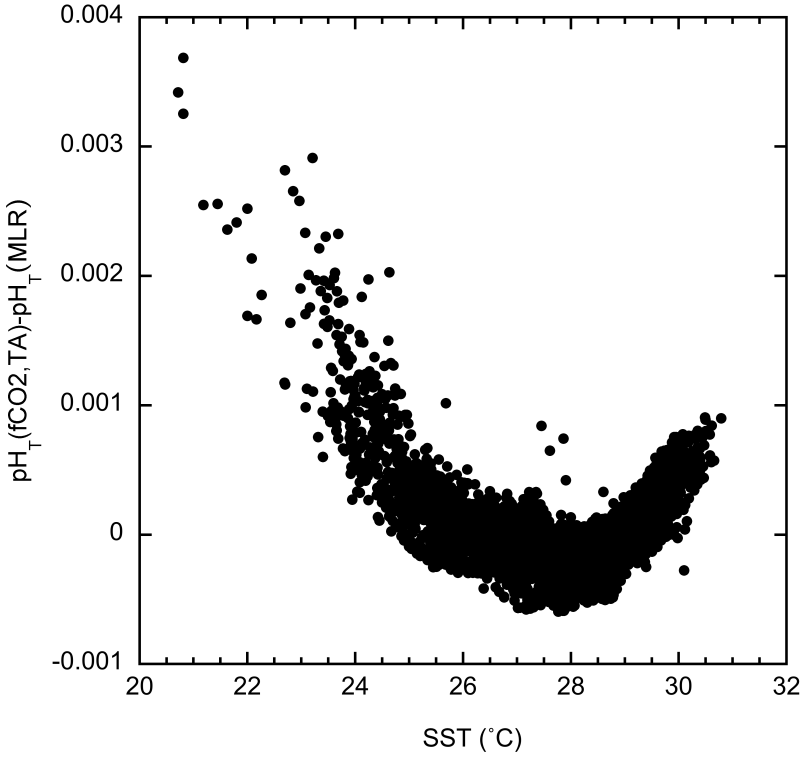
0.004
0.003
0.002
0.001
0
-0.001
20
22
24
26
28
30
32
pH_T(fCO2,TA)-pH_T(MLR)
SST (˚C)

Fig. 6

865